universität wien

MASTERARBEIT / MASTER'S THESIS

Titel der Masterarbeit / Title of the Master's Thesis

„Investigating multienzyme-like activity of High entropy nanoparticles“

verfasst von / submitted by

Mohamed Hossam Mohamed HASSAN

angestrebter akademischer Grad / in partial fulfilment of the requirements for the degree of

Magistra pharmaciae (Mag.pharm.)

Wien, 2023 / Vienna, 2023

Studienkennzahl lt. Studienblatt / degree programme code as it appears on the student record sheet:	UA 066 605
Studienrichtung lt. Studienblatt / degree programme as it appears on the student record sheet:	Masterstudium Pharmazie
Betreut von / Supervisor:	**Univ.-Prof. Dr. Lea Ann Dailey**

Acknowledgment

I would like to express my deepest gratitude to Prof. Lea Ann Dailey for her unwavering support and guidance throughout my thesis journey. Her insightful feedback and expert advice have been instrumental in shaping my research and enhancing its quality.

My sincere appreciation and gratitude to Thuong Phan, my co-supervisor, for his invaluable guidance, support, and insightful feedback throughout my thesis. I am grateful for his mentorship and encouragement, which have been a constant source of motivation and inspiration.

I would like to express my deepest appreciation to Dr. Gianluca Bello and all my colleagues in Prof. Dailey's group for their support and cooperation throughout my thesis journey.

Also, I would like to take this opportunity to express my heartfelt thanks to my family and friends for their unconditional love, support, and encouragement throughout my academic journey. Their unwavering belief in me, even during challenging times, has been a driving force in my success. I am grateful for their constant encouragement and motivation, which have pushed me to strive for excellence. I cannot thank them enough for their love and support.

Finally, I would like to extend my gratitude to the entire team at St. Severinus Pharmacy for their support and understanding. Their professionalism and dedication to their work have been an inspiration to me.

Thank You

Mohamed H. M. HASSAN

Table of Contents

List of figures

0.987, 0.981, 0.978) for HEN, Fe_eO_4-NP, and HRP respectively, representing the double reciprocal of the velocity and TMB concentration. (V_0) represents the reaction velocity and [TMB] is the concentration of TMB. Values represent the mean ± standard deviation of n=3 replicates.

Figure 11. Fluorescence spectrum from 400 – 480 nm for 20, 40, and 80 µg/ml HEN, 1 M of H_2O_2, and 0.625 mM sodium terephthalate compared with control (absence of HEN) shows no difference in spectrum between all tested concentrations and control, which indicates the absence of hydroxyl radical. Values represent the mean ± standard deviation of n=3 replicates.

Figure 12. The reaction rate of 40, 80, and 160 µg/ml of HEN in the presence (green) and absence (blue) of p-BQ with TMB in presence of H_2O_2, showing a negative control (without HEN) show the effect on the reaction and exclude any interference of p-BQ to the reaction rate. Values represent the mean ± standard deviation of n=3 replicates.

Figure 13. shows a Spectrophotometric analysis of Cytochrome C involved in the electron transfer process of the Peroxidase reaction, as the Black line shows reduced Cytochrome C with two peaks at 520 and 550 nm, on the other hand, the red line shows only one Peak at 530 nm.

Figure 14. (a) The graph shows the percentage of fluorescence reduction over time for four concentrations of HEN (20, 40, 80, and 160 µg/ml) in comparison to negative and positive (with native catalase enzyme) control. Values represent the mean ± standard deviation of n=3 replicates. (b) The catalase-like activity of HEN appears in the production of oxygen bubbles as a result of H_2O_2 decomposition.

List of tables

List of abbreviations

- POD- Peroxidase
- HEO- High entropy oxide
- HEN- High entropy nanoparticle
- HEM- High entropy metal
- HEC- High entropy ceramic
- CNT- Carbon nanotubes
- CQD- Carbon quantum dots
- CND- Carbon nano dots
- TMB- 3,3',5,5' tetramethyl benzidine
- SOD- superoxide dismutase
- NP- nanoparticle
- HRP- Horseradish peroxidase
- MOF- Metal-organic framework
- V_0- initial velocity
- V_{Max}- Maximum catalytic reaction velocity
- [S]- Substrate concentration
- K_M- Michaelis constant
- A – Absorbance
- ε- Extension coefficient (molar absorptivity coefficient)
- TA- Terephthalic acid
- NaTa- Sodium terephthalate
- Na Ac- Sodium acetate
- (Eu-Tc)- europium tetracycline complex
- ($OH^{\bullet}$)- Hydroxyl radical
- ($O_2^{\bullet -}$)- Superoxide radical
- GPx- Glutathione peroxidase enzyme
- ROS- Reactive oxygen species
- Ce-NP nanoceria (cerium nanoparticles)
- O_2^1- Singlet oxygen
- LSRP- localized surface plasmon resonance
- CDT- chemo-dynamic therapy
- DMSO- Dimethyl sulfoxide
- H_{mix} - Enthalpy of Mixture
- S_{mix} - The Entropy of Mixing
- xi - The atomic fraction
- p-BQ – 1,4 Benzoquinone
- MIP-AuNPs - Molecularly imprinted gold nanoparticles

Abstract

In the past two decades, there has been a growing interest in studying nanozymes due to their enzyme-like catalytic activities, demonstrating their potential application in the industrial, biochemical, analytical, and pharmaceutical fields. Nanozymes are classified based on their fabricated materials and their specific catalytic activities. Some nanozymes exhibit single or multienzyme-like activities, such as POD- (peroxidase), catalase-, oxidase, or superoxide dismutase-like activities. These nanomaterials possess unique physical, chemical, and electrical properties that lead to different mechanisms of their catalytic activity, such as electron transfer processes or free radical production.

One promising class of nanomaterials with a high potential for catalytic activity is high-entropy oxides (HEOs). HEOs as a class of high-entropy nanoparticles (HEN) are modern nanomaterials with diverse applications and the ability to lower reaction energy rates. Therefore, this thesis investigates the multienzyme-like activity of HEO, and compares their peroxidase-like activity to other well-studied nanozymes, such as Fe_3O_4 nanoparticles and natural enzyme Horseradish peroxidase (HRP), using Michaelis-Menten Kinetics. The study also investigates the mechanism of peroxidase-like activity and the detection of the catalase-like activity of HEOs.

In the reaction condition of this study, HEN exhibited a 2.6 folds higher affinity towards TMB than native HRP. In addition, this material accelerated the reaction speed by 3.6 folds compared to Fe_3O_4-NP. Regarding the reaction mechanism, it turned out that the oxidation of the peroxidase-substrate is driven by the electron transfer, rather than the formation of free radicals such as hydroxyl radicals or superoxide radicals. Interestingly, the material exhibited catalase-like performance at the concentration of 80 µg/ml similar to 0.1 mg/mL of native catalase during the decomposition of H_2O_2. These findings contributed to the understanding of HEN regarding enzyme-like activity and further supported their use in biomedical fields.

Kurzfassung

Nanozyme wurden in den letzten Jahrzehnten zunehmend untersucht, was auf die Bedeutung von enzymähnlichen Nanomaterialien nicht nur im industriellen Bereich, sondern auch in den biochemischen, analytischen und pharmazeutischen Bereichen hinweist. Nanozyme werden aufgrund ihrer hergestellten Materialien und ihrer spezifischen katalytischen Aktivitäten klassifiziert. Einige Nanozyme zeigen ein- oder mehrere enzymartige Aktivitäten, wie z.B. POD-, Katalase-, Oxidase- oder Superoxid Dismutase-ähnliche Aktivitäten. Diese Nanomaterialien besitzen einzigartige physikalische, chemische und elektrische Eigenschaften, die zu verschiedenen Mechanismen ihrer katalytischen Aktivität führen, wie z.B. Elektronentransferprozesse oder die Produktion freier Radikale.

Ein vielversprechendes Nanomaterial mit hohem Potenzial für katalytische Aktivität sind Hochentropieoxide (HEOs). HEOs sind moderne Nanomaterialien mit vielfältigen Anwendungen und der Fähigkeit, Reaktionsenergie-Raten zu senken. Deshalb untersucht diese Arbeit die Multienzyme-ähnliche Aktivität von HEO und vergleicht ihre Peroxidase-ähnliche Aktivität mit anderen gut untersuchten Nanozymen wie Fe_3O_4-NP und dem natürlichen Enzym HRP unter Verwendung von Michaelis-Menten-Kinetik. Die Studie untersucht auch den Mechanismus der Peroxidase-ähnlichen Aktivität und die Erkennung der Katalase-ähnlichen Aktivität von HEOs.

Unter den Reaktionsbedingungen dieser Studie zeigte HEN eine 2,6-fach höhere Affinität gegenüber TMB als das native HRP. Darüber hinaus beschleunigte dieses Material die Reaktion um das 3,6-fache im Vergleich zu Fe_3O_4-NP. In Bezug auf den Mechanismus stellte sich heraus, dass der Elektronentransferprozess bei der Oxidation des Substrats eine Rolle spielt, anstatt die Bildung von freien Radikalen wie Hydroxylradikale oder Superoxid-Radikale. Darüber hinaus war es interessant, dass das Material auch eine Katalase-ähnliche Aktivität besaß, wobei eine Konzentration von 80 µg/ml HEN denselben Effekt wie 0,1 mg/ml native Katalase bei der Zersetzung von H_2O_2 zeigte. Diese Erkenntnisse trugen zum Verständnis von HEN hinsichtlich enzymähnlicher Aktivitäten bei und legten nahe, dass sie in der Biomedizin Anwendung finden können.

I. Introduction

1. Overview of nanozymes

Enzymes are biocatalysts that are available in living organisms, such as animals, plants, and microorganisms, which purpose is to accelerate biological reactions within the cells by lowering the activation energy to efficiently maximize cell homeostasis [1]. Unfortunately, natural enzymes have many limitations when it comes to their alternative applications, such as their ease of denaturation due to low stability in harsh conditions, such as pH or temperature susceptibility, their high cost of synthesis, and the laborious preparation and recycling [2]. These drawbacks have led to extensive research for alternatives to natural enzymes or ways to enhance their application.

Nanozymes are considered a practical alternative to natural enzymes due to the various advantages they provide, such as high stability at high temperatures and in different acidic or alkaline media, ease of mass production, low cost of synthesis, long-term storage, comparable catalytic activity to natural enzymes, multienzyme mimetic activity, and controllability of catalytic activity through external stimuli [3–5].

In the past few years, nanozymes have been extensively researched and applied in various fields, such as biosensors, disease diagnosis, and in vivo monitoring and therapy, which reflects the importance of enzyme-mimetic nanoparticles [6]. The term "nanozymes" was first introduced by Scrimin in 2004 and describes the catalytic activity performed by nanoparticle materials [7]. Finally, in 2007, Gao *et al*. discovered the intrinsic peroxidase-like activity of Fe_3O_4 nanoparticles [8], which opened the gate to researchers for more enzyme-like activity materials.

Nanozymes are materials measured in one or more of the dimensions of their particles in the nanoscale (≤100 nm) regardless of the shape of the particles, that exhibit enzyme-like activities.

Nanomaterials, that possess enzyme-like activities can be categorized as antioxidant mimetics, which scavenge free radicals, and pro-oxidant mimetics, which can produce free radicals. Depending on the mechanism of activity for each nanomaterial, the activity can be utilized in a wide range of applications for diagnosis, immunoassay, and therapy.

In this section, the most commonly studied enzyme-like activities would be covered (peroxidase, catalase, oxidase, and superoxide dismutase), focusing on the mechanism of catalytic reaction, parameters that influence the activity, and tuning the conditions and methods for activity enhancement.

2. Classification of Nanozymes based on material

Nanozymes have been recently more developed and categorized according to the raw materials, with which they are fabricated. As shown in Scheme 1, nanozymes could be represented in four main types; Metal-based, nonmetal-based, metal-organic framework, and alternative nanozymes. We will go through each type of these categories briefly mentioning the main differences and describing their enzymatic activity.

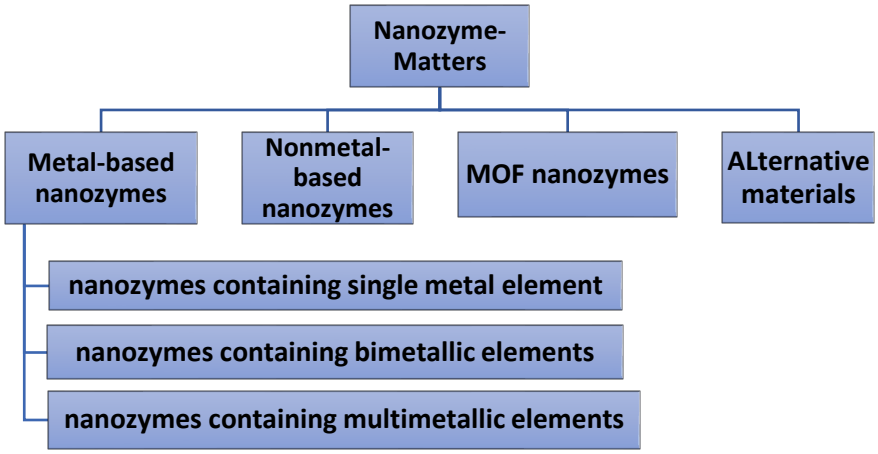

Scheme 1. The main classification of nanozyme matters.

2.1. Metal-based nanozymes

More than 40 elements have been used to prepare nanozymes based on metals such as Fe, Cu, Ni, Mo, Pd, Ag, Au, and more nanomaterials could exist as nanometals, metal oxides, or metal-metal composites. Transition metals, especially, can coordinate bonds with substrates, forming a lower energy transition state, hence reducing the activation energy of the whole reaction [9–11].

Metal-based nanozymes can be subcategorized into single metal-, bimetal- or multimetal-containing nanozymes. For instance, as a single metal-based nanozyme, Fe_3O_4-nanoparticles (NP) have been studied and modified since the discovery of their intrinsic enzyme-like activity [8]. An example of a derivative of previous nanozymes is the bimetal nanozyme $MnFe_2O_4$ which shows oxidase-like activity with catalytic efficiency of 2.21×10^9 M^{-1} s^{-1} [12].To prepare a highly active and stable nanozyme with higher selectivity, multiple metals nanozyme have been taken into consideration due to their synergistic effect [13]. Zhang *et al*. reported the activity of a Pt/Pd/Mo trimetallic nanozyme, which possesses higher catalytic activity and improved selectivity in the physiological environment compared to single metal nanoparticles [14], therefore, it is suggested that the increased catalytic activity is due to the increased active sites.

2.2. Nonmetal-based nanozymes

Generally, nonmetal substances are not involved in the catalytic process due to the saturation of their orbits which makes them less reactive. However, the fast development of nanoscience allowed nonmetallic nanozymes to be structured in a catalytically active way. For example, the carbon nanotubes (CNT) show their catalytic activity after the treatment with strong acids, which produced functional groups on the surface of the CTN, these groups are responsible for this catalytic activity [15]. Due to the chemical and physical properties of carbon nanomaterials, they have been widely used as catalysts such as graphene oxides (GOs)[16], carbon quantum dots (CQDs)[17], and carbon nanotubes (CNTs)[18]. Another example of nonmetal nanozymes is the synthesis with polymers such as melanin, which shows a superior ROS scavenging property due to polydopamine reported by Marcod'Ischia *et al.,* where the atypical structure of Melanin exhibits multi anti oxidative activity in addition to anti-inflammatory actions[19].

2.3. Metal-organic framework (MOF) nanozymes

Metal-organic framework-based nanozymes are considered to set the beginning of a new era in nanozymes development. They are porous materials with large surface areas, adjustable pore size, easy to be modified, they possess different shapes, and many unsaturated metal sites. Although they contain metals, their physical and chemical properties are completely different from the traditional metal nanozymes, as MOF contains a larger specific surface area, adjustable pore size, and shape, easier to be modified, and possesses a larger number of unsaturated metal sites [20]. An example of a MOF-based nanozyme is ultrasmall AuNP grown on 2D metalloporphyrin MOF nanosheets, which showed a high peroxidase mimic activity [21].

2.4. Alternative nanozymes

During the investigation of various nanozymes and their activities, another nanomaterial class exhibited compelling enzyme-like activity. Wang *et al*. reported the ability of hemin-loaded mesoporous silica nanoparticles to remove the intracellular reactive oxygen species (ROS) [22], where the hollow nanoparticles showed 3.5-fold higher activity of ROS removal than solid NPs made of the same materials. This work encouraged other researchers to further investigate such materials, for instance, Wang *et al*. presented a core-shell supramolecular hybrid nano-gel via oligopeptides around Iron oxide NP [23]. Another example introduced by Zhang *et al*. reported that the synthesized transformable hybrid semiconducting polymers showed enzyme-like activity [24].

3. Enzyme-like activity and mechanism of nanozymes

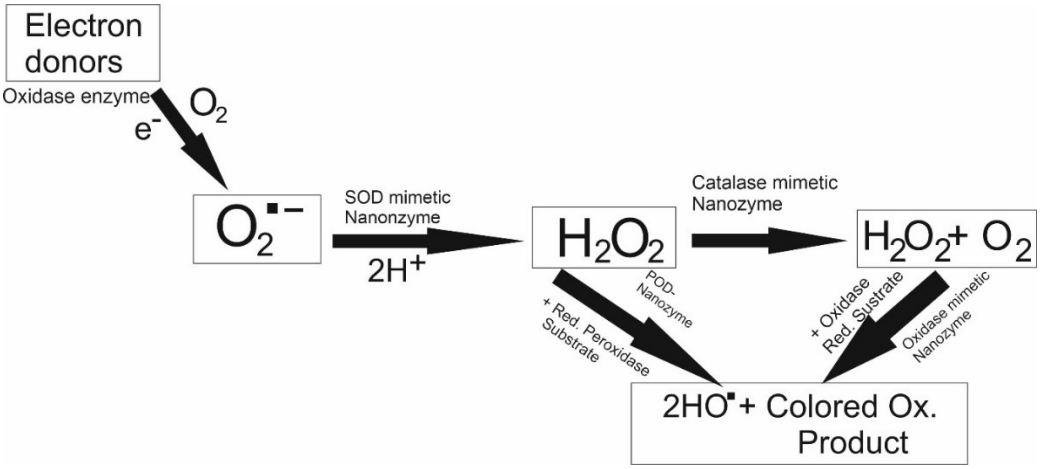

Figure 1. An exemplary representation of possible redox reaction connections involving enzymes and nanozymes showing the effect of Oxidase as an electron donor, Superoxide dismutase mimetic enzyme effect to produce H_2O_2, catalase mimetic nanozyme on H_2O_2 to produce H_2O and O_2 that could produce hydroxyl radical as a result of oxidase mimetic nanozyme activity in presence of reduced oxidase substrate, and effect of Peroxidase mimetic nanozyme on reduced peroxidase substrate in presence of H_2O_2 to produce a colored oxidized product and H_2O.

3.1. Anti-oxidant mimetics

Antioxidants in biological systems have the role of scavenging potentially harmful free radicals, that are produced through different biochemical reactions occurring in the human body. Examples of anti-oxidant enzymes in mammalian systems are superoxide dismutase (SOD) enzyme, catalase, glutathione peroxidase, and glutathione reductase.

In this section, SOD mimetic nanozyme and Catalase mimetic nanozyme will be detailed mentioning enzyme mimetic examples for each activity.

i. Superoxide dismutase mimetic nanozyme:

SOD mimetic nanozyme shows antioxidant ability through scavenging superoxide anions in the system. As shown in Figure 1, the SOD enzyme reacts with superoxide radicals, which might cause harmful effects in mammalian cells. Scheme 2 shows the scavenging reaction of SOD mimetic NP which eliminate [$O_2^{\bullet -}$] free radical and produces hydrogen peroxide and molecular oxygen instead.

$$2O_2^{\bullet -} + 2H^+ \xrightarrow{SOD} O_2 + H_2O_2$$ *Scheme 2*

There are a few nanozymes, that show SOD mimetic activity and one of them is nanoceria (Ce-NP) [25,26]. Ce-NP shows significant evidence of SOD mimetic activity in presence of $O_2^{\bullet -}$

and catalase activity in the case of H_2O_2 presence. The ratio of Ce^{+3}/Ce^{+4} on the surface atoms on nanoceria plays a vital role in defining the nanozyme activity, where the high ratio shows SOD mimetic activity, whereas the lower Ce^{+3}/Ce^{+4} ratio exhibits catalase activity [27].

ii. Catalase mimetic nanozyme

After the reaction of superoxide dismutase enzyme with superoxide radical [$O_2^{\bullet -}$] as shown in Figure 1, hydrogen peroxide accumulated in cells, which may lead to harmful consequences due to oxidative stress. Although hydrogen peroxide itself is more stable than free radicals and ROS (reactive oxygen species), it is documented that H_2O_2 might be involved in biological signaling and undergoes what is called the Fenton reaction in presence of transition metal ions to form hydroxyl radical, that could be extremely destructive to the human cell [28].
Hydrogen peroxide accumulation in absence of natural catalase enzymes is linked to the development of autoimmune diseases such as Diabetes mellitus or vitiligo. Therefore, the activity of the catalase enzyme is to break down H_2O_2 and turn it into less detrimental water and molecular oxygen as shown in Scheme 3.

$$2H_2O_2 \xrightarrow{Catalase} 2H_2O + O_2$$ *Scheme 3*

For such reasons, research focuses on alternative catalase enzyme mimetics with enhanced stability and affordable cost of synthesis. The catalase mimetic activity has been reported experimentally in some nanozyme such as iron oxide, cobalt oxide, gold nanoparticles, and as mentioned before in SOD mimetic subsection cerium oxide [29–32].
Recent studies show that catalase mimetic nanozyme Ce-NP could protect hepatic cells from genetic damage or cytotoxicity induced by the accumulation of hydrogen peroxide by protecting the hepatic cells from exposure to 3-aminotriazole, which cause hepatic cellular apoptosis due to high H_2O_2 concentration inside the cell [33]. Iron oxide nanoparticles show significant catalase-like activity besides peroxidase-like activity, these enzymatic activities are pH dependent, as it shows the catalase-like activity in [pH=7,4], while in an acidic medium with [pH=4], the peroxidase-like activity appears, which will be discussed later in Peroxidase like activity nanozymes [34].

3.2. Pro-oxidants mimetics

Pro-oxidant nanozymes are enzyme-like nanoparticles, that induce oxidative stress or inhibit anti-oxidant systems inside living cells by producing free radicals that could be harmful to cells and might lead to cell death (apoptosis). This pro-oxidant activity is similar to that shown by paracetamol or methotrexate in hepatic cells, where free radicals are generated. Many transition metals such as copper and iron show a similar activity through Fenton reaction or Haber-Weis reaction. Such activity has been recently reported for NPs containing such metals [35].

i. Oxidase mimetic nanozymes

Oxidase enzymes catalyze the oxidation reaction of the substrate in presence of oxygen, into water or hydrogen peroxide. The production of H_2O_2 or free radicals can be exploited by oxidase enzymes and oxidase-like nanozymes for the development of efficient colorimetric reactions used in diagnostics [36–38]. Scheme 4 shows a representation of Oxidase mimetic activity.

$$AH + O_2 \xrightarrow{Oxidase} A + H_2O$$

$$AH + O_2 + H_2O \xrightarrow{Oxidase} A + H_2O_2$$ *Scheme 4*

Oxidase mimetic nanozymes have been used to detect lung tumor cells such as Ce-NPs conjugated with poly acrylic acid and functionalized with folic acid. This conjugate is able to selectively detect the high expression of folate receptors in lung tumor cells [39]. For instance, a study showed that MnO_2 nanowires conjugated with antibodies show oxidase-like activity, that could be used for the development of immunoassay of sulfate-reducing bacteria with high selectivity and sensitivity towards bacteria [40].

Overall, oxidase enzymes and oxidase mimetic nanozymes have emerged as important tools in the detection of various biological and chemical molecules. With their unique properties, they offer a promising approach for the development of highly sensitive and selective biosensors for various applications, including medical diagnosis, environmental monitoring, and food safety.

ii. Peroxidase mimetic nanozymes

Peroxidase enzymes are considered natural detoxifying agents catalyzing the conversion of H_2O_2 into molecular water as shown in Scheme 5, in addition to their ability to facilitate the eradication of pathogens through myeloperoxidase activity, which utilizes H_2O_2 to produce Hypochlorous acid and other moieties to kill the pathogen [41].

$$2AH + H_2O_2 \xrightarrow{Peroxidase} 2A + 2H_2O$$ *Scheme 5*

One of the most studied catalytic enzymes is Horse-radish peroxidase (HRP), which has been applied in clinical chemistry and bioanalytical chemistry by converting the colorless reduced substrate to an oxidized colored product. This enzyme is also used in our studies as a standard for peroxidase activity. Gao et. al in 2007 reported, that the peroxidase-like activity of iron oxide NP was 40 folds higher than the natural HRP. In addition, these particles showed a higher substrate affinity (K_M) towards the peroxidase substrate TMB as well as higher stability over a wide range of pH and temperature [8].

Following Gao *et al*. work, other several studies investigated the intrinsic peroxidase activity of iron oxide NP and its application in the detection and sensing of other materials such as hydrogen peroxide and Glucose [42,43]. The results of such studies created an interest in the special properties of iron oxide nanoparticles specifically and discovered new nanometals

with the same characteristics. Other iron-metal combinations such as Fe-S nanosheets have been studied, showing greater peroxidase activity because of the large surface area[44].

Further investigations reported the peroxidase-like activity of other nanometals such as Au-NP whose activity improved by up to three folds in presence of negatively charged ATP and has been used in detecting several biomolecules [45]. Many other bimetallic compositions have been studied as peroxidase mimetics, which illustrates the importance of discovering new nanozymes that can catalyze biological reactions. Some examples of peroxidase-like nanozymes are V_2O_3, by Zhang *et al*. [46], and ZrO_2, presented by Pietrzyk *et al*. [47]

Not just the composition of nanoparticles influences the catalytic activity. Later on, in 2007, Gao *et al*. showed that different sizes of iron oxide NP (30, 50, and 300 nm) have different peroxidase activity. Moreover, different nanostructures have a significant influence on the peroxidase activity of nanozymes, as shown in the paper of Dutta *et. al* 2012 which reports a greater peroxidase activity of Fe-S in a nanoneedle form compared to spherical shape [48].

3.3. Mechanism involved in enzyme-like activity mimetics

The catalytic activity of nanozymes relies on a variety of mechanisms that are not yet fully understood. Nevertheless, a multitude of studies has focused on the mechanism for different types of nanozymes through experimental research. This section will delve into the most prevalent mechanisms involved in the catalytic activity of nanozymes and will describe more in detail the Peroxidase and Catalase processes, as they are the focal point of this research.

1. Peroxidase-like nanozymes mechanisms

The peroxidase-like nanozyme in presence of hydrogen peroxide oxidizes the substrate and produces a colored oxidized product. This activity can be exploited *in vitro* assays for the detection of biomolecules or in other diagnostic applications. Generally, the catalytic activity of peroxidase-like- nanozyme could be categorized into two different mechanisms [49,50];

1- Free radicals production such as hydroxyl radical ($OH^{\bullet}$) or Superoxide anion radical ($O_2^{\bullet -}$).
2- Electron transfer process.

The peroxidase-like activity of nanozymes is well documented and is possibly based on Fenton or Fenton-like reactions. After the adsorption of H_2O_2 on the surface of nanozyme, the bond between O-O breaks up producing two hydroxyl radicals $OH^{\bullet}$, which are stabilized by electron transfer interaction [51]. The hydroxyl radical is responsible for the oxidation of the substrate into colored products [52,53].

Other than the Fenton-like reaction mechanism, some nanozymes such as Ag/Au [54] may present a peroxidase-like activity by electron transfer, where the nanozyme act as a mediator to facilitate the electron transfer between hydrogen peroxide and the substrate to be oxidized [55,56]. Scheme 6 displays a reaction of electrons, donated from the substrate to the nanozyme, generating a high electron density of nanozyme. Finally, the peroxidase substrate

is oxidized, while hydrogen peroxide, as an electron acceptor, is reduced into water molecules.

$$H_2O_2 + 2e^- + 2H^+ \xrightarrow{POD} 2H_2O$$ *Scheme 6*

2. Catalase nanozyme mechanism

Some nanozymes show catalase mimetic activity, as they have the ability to turn hydrogen peroxide into H_2O and molecular oxygen O_2. This catalytic reaction mechanism depends mainly on the structure of the nanoparticle. Although the catalase-like mechanism is not fully understood, two pathways might explain the catalase-like activity of nanozymes. Since there are two different bonds in H_2O_2 (O-O and H-O bonds), the mechanism could be categorized into homogeneous (between O-O) and heterogenous (between H-O) depending on the bond broken [57].

A suggested mechanism of catalase-like reaction for nanoceria (Ce-NP) is proposed as the redox cycle between Ce^{3+} and Ce^{4+} on the surface of the nanozyme. Some studies showed that H_2O_2 oxidizes Ce^{3+} into Ce^{4+} in a reversible oxidation reaction, in a process that is not yet well defined. Recently, an additional mechanism has been proposed as H_2O_2 might have the ability to reduce Ce^{4+} in nanoceria into Ce^{3+}, the H_2O_2 would be oxidized to molecular oxygen in a similar reaction of Catalase-like enzyme as shown in Figure 2 (steps 1-4) [58].

3. Oxidase nanozyme mechanism

The oxidase-like activity of enzymes shown by many nanoparticles describes the ability to catalyze the oxidation reaction of many substrates in presence of O_2 to produce an oxidized product of substrate and hydrogen peroxide, therefore these nanozymes could be utilized in vitro in oxidase substrates detection, for example, the detection of sulfite and L-cysteine by oxidase-like hollow $MnCo_2O_4$ nanofibers [59]. The mechanism of the oxidase-like reaction of nanozyme depends on the structure of the nanoparticle (nanozyme) and the substrate [60]. For instance, nanoceria shows oxidase-like activity through the redox cycle of Ce^{3+}/Ce^{4+} and $O_2^{\cdot -}$ production, initially O_2 adsorbed on the surface of nanoceria and converted into $O_2^{\cdot -}$, as a result, the substrate gets oxidized simultaneously while Ce^{4+} on the surface of nanoceria reduced to Ce^{3+}. Finally, Ce^{3+} is re-oxidized into Ce^{4+} again through formulated ($O_2^{\cdot -}$) [61]. Another oxidase-like possible mechanism was reported by Long *et al*., Pd-NP shows oxidase-like activity through adsorbing O_2 on the surface, which is converted into actively singlet oxygen [O_2^1] by electron transfer, this generated O_2^1 is responsible for the oxidation of substrate and oxidase-like activity of many noble metals such as Pd-NP [62]. Furthermore, the oxidase-like activity of Mn nanoparticles suggested a mechanism, as O_2 converted into ($O_2^{\cdot -}$), which converted partially into H_2O_2, that decomposed subsequently into $OH^{\bullet}$ in presence of Mn ions. The formed $OH^{\bullet}$ is responsible for the oxidase-like activity of Mn-NP [63].

4. Superoxide dismutase nanozyme mechanism

SOD acting like nanoparticles gained their importance from their ability to eliminate the harmful $O_2^{\bullet -}$ radicals and turn them into H_2O_2 and O_2, although the mechanism of this activity is structure dependent. The most accurate suggested mechanism of SOD-like nanozymes, especially metal, metal oxide, metal carbides, and metal sulfides of Pt, Au, Co, Ni, and others is the protonation of $O_2^{\bullet -}$ then adsorption and rearrangement of the formed $HO_2^{\bullet}$ on the surface of the nanozyme. Once $HO_2^{\bullet}$ is adsorbed on the surface of the metal it converts into O_2 and H_2O_2, as $HO_2^{\bullet}$ contains a low potential energy profile.

For instance, the nanozymes attract the radical anions electrostatically on their surface, then the dismutation of the substrate [64]. Another mechanism has been proposed based on the redox cycle (as shown in the catalase-like nanozyme mechanism), where the activity of nanoceria depends on the fraction of Ce^{3+} ions. The Ce^{3+}/Ce^{4+} ratio somehow controls the SOD activity, where Ce^{3+} needs to be oxidized to $Ce^{4+,}$ and on the other hand, the superoxide is reduced to H_2O_2 and molecular oxygen as shown in Figure 2 (steps 5-7). The restoration of the reduction state for the metal is followed in this case of nanoceria spontaneously by not fully understood mechanism [58]. in conclusion, superoxide is attracted at the surface of the nanozyme reacting with protons producing H_2O_2 on the surface, and this mechanism is found by other nanometals such as Fe- and Mn- SOD-like nanozymes [65].

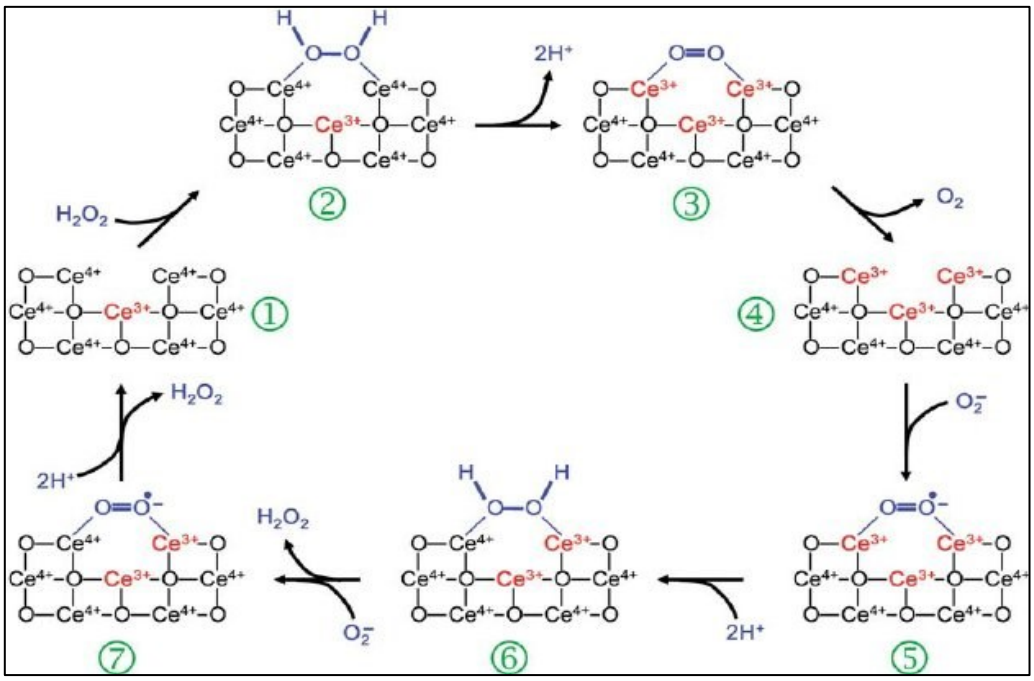

Figure 2. A model reaction represents the redox cycle that occurs between Ce^{4+} on the surface of nanoceria and H_2O_2, followed by the reduction of Ce^{4+} into Ce^{3+} and producing protons and then molecular oxygen leaving the molecule, which mimics catalase activity (steps 1- 4). The reaction of superoxide at step (5) with nanoceria was generated at the end of the reaction H_2O_2 and oxidized Ce^{4+} on the surface of nanozyme. Adopted from Celardo et al. [58]*, copyright from The Royal Society of Chemistry 2011.*

4. Parameters influencing the catalytic activity of nanozymes

Although nanozymes are believed to be chemically and biologically inert, some parameters have been reported to influence their enzymatic-like activity such as pH, temperature, and substrate concentration. Here we shortly describe some of such findings.

4.1. pH of the medium

The pH of the medium is an important parameter that affects the catalytic activity of nanozyme. Wei et. al. reported that iron oxide NPs show a faster peroxidase-like activity in an acidic medium (pH=4) than in a basic medium, due to the variation of Fe^{2+}/Fe^{3+} ions ratio in solution, in addition to the leaching of Fe ions from the NPs structure [42]. Similarly, Ag-based nanozymes peroxidase-like activity increases as the medium shifts towards acidic pH [66].

4.2. Temperature

The efficacy and stability of nanozyme could be affected by the different reaction temperatures. For example, Gao *et. al* reported that iron oxide NP compared with HRP and both showed higher catalytic activity at 40 °C, despite the better stability of iron oxide nanozymes within the range of (25 to 60 °C) [8]. Another investigation carried out on Ag nanozyme at three different temperatures (15, 25, and 35 °C) showed higher catalytic activity at room temperature (25 °C) [67]. That means, although nanozyme are stable in a wide range of reaction temperatures, they exhibit their highest activity in a specific temperature.

4.3. Substrate concentration

The peroxidase-like reaction of nanozymes requires the presence of hydrogen peroxide to complete the reaction and generate the oxidized product at the end of the reaction. Liu *et al*. showed that Ag nanozymes activity increases proportionally up to a substrate/nanozyme molar ratio of 7.3. Adding more H_2O_2 substrate above such a threshold results in a decrease in activity showing a "hump-shaped relationship" [66]. Interestingly, this behavior has also been reported for HRP [68]. A possible explanation of such phenomena could be due to the competitive inhibition of excess substrate absorbing onto the nanozymes surface.

5. Strategies to improve the catalytic activity of nanozymes

Several studies focused on the improvement of enzyme-like NPs in terms of enhancement of substrate selectivity and increase in the catalytic reaction rate of nanozyme.
The enhancement of the catalytic activity of nanozymes can be attributed to several factors including an increase in the surface area of nanomaterials to provide a larger number of active sites for the reactants, size, shape, and composition, which can affect the reaction kinetics and selectivity. Additionally, the nanomaterials' electronic properties, such as their conductivity and redox potential, can also contribute to their performance.
Modification of nanozymes could be achieved in five different ways:

5.1. Nanozyme surface modification:

Gold nanoparticles (Au-NP) with peroxidase-like activity can be enhanced via surface chemistry by introducing carboxyl groups on their surface, which increases their affinity towards the substrate and facilitates the reaction kinetics [69]. Similarly, carbon-based nanomaterials, such as graphene oxide and carbon nanotubes, have also been reported to exhibit peroxidase-like activity, which can be enhanced by introducing defects on their surface. A study by Wu *et al*. showed that the catalytic activity of graphene oxide can be enhanced by introducing oxygen-containing functional groups on its surface, which creates more active sites for the substrate to bind and undergo catalysis [70].

5.2. Nanozymes size, shape, and morphology improvement:

Nanozymes with other types of catalytic activity than the peroxidase-like one have also been reported to show enhanced performances due to specific modifications. For instance, Gold metal-organic frameworks (MOFs) with oxidase-like activity can be enhanced by controlling their size as the smaller the particle size (down to 3-5 nm), the higher the surface/volume ratio compared to allowing for a greater number of active sites [72].

The morphology and shape of nanozyme also play an important role in determining their catalytic activity. For instance, Mugesh and colleagues compared the multi-enzymatic activity (catalase, SOD- and Glutathione peroxidase GPx) of differently shaped Mn_3O_4-NP (nanoflowers, flakes, cubes, and hexagonal plates) funding out a greater catalytic activity for nanoflowers shape over other morphologies for all three catalytic activities [73].

5.3. External excitation such as localized surface plasmon resonance (LSPR):

An additional catalytic mechanism enhancement of Peroxidase-like nanozyme based on “Hot Electron” generation using localized surface plasmon resonance (LSPR) excitation was performed, where the generated hot electrons decompose H_2O_2 producing $OH^{\bullet}$ free radical and OH^- anions. The hydroxyl radical possesses a high catalytic activity that oxidizes the peroxidase substrate.

LSPR excitation generates holes (nanoscale gaps or voids in a thin metal film, which are intentionally created to enhance the sensitivity of the LSPR sensor) in addition to hot electrons, these holes are scavenged by electron donors through three different pathways as shown in Figure 3, the scavenging of holes reduces the probability of recombination between hot electrons and holes, thus maintaining higher catalytic activity.

First channel: holes are consumed by OH^- anions, generated through H_2O_2 cleavage, the second channel: is depletion through water molecule oxidation, and the third channel is through additional electron donors such as Ethanol [74]. In conclusion, the recombination of hot electrons and holes could be inhibited using scavengers, leading to fast cleavage of H_2O_2 and increasing the reaction rate significantly.

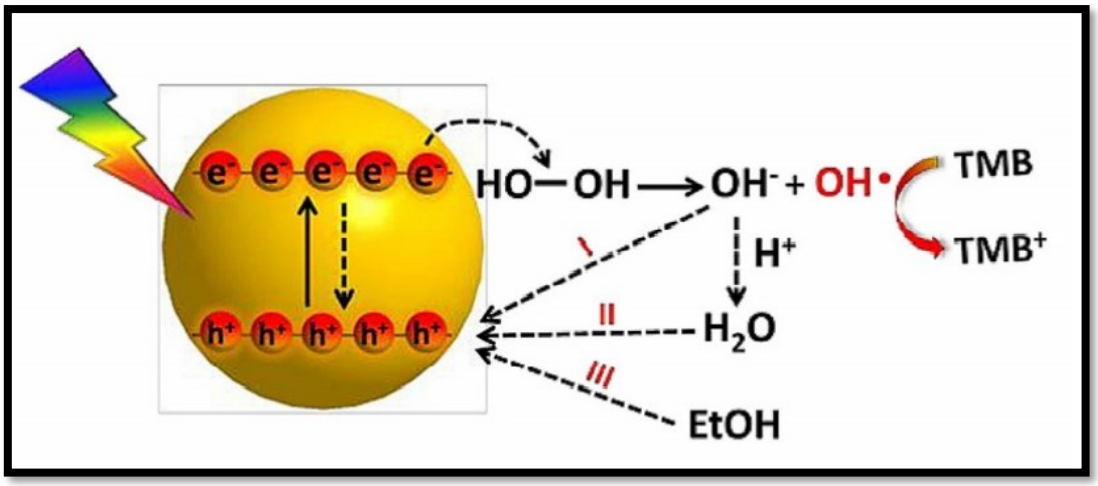

Figure 3. An illustration of a suggested peroxidase enzyme-like activity mechanism of Au-NP based on the generation of the hot electron with three different pathways under LSPR. Adopted from wang et al. [74] *Copyright 2017, Wiley-VCH.*

5.4. Molecular imprinting technique:

Molecular imprinting involves the creation of cavities, or imprints, in the nanomaterial's structure, which is complementary to the target substrate's size, shape, and functional groups, and can be used to enhance the nanozymes selectivity [75]. For example, Gao *et al.* reported the creation of molecularly imprinted gold nanoparticles (MIP-AuNPs) with peroxidase-like activity for the selective detection of prostate-specific antigen (PSA). The MIP-AuNPs exhibited a 10-fold higher catalytic activity towards the oxidation of 3,3',5,5'-tetramethylbenzidine (TMB) in the presence of PSA, compared to non-imprinted AuNPs [76]. Similarly, Wu *et al*. reported the higher activity of molecularly imprinted carbon nanodots (CNDs) compared to non-imprinted CNDs for the detection of glucose [77].

5.5. Composition modification (Metal doping and complexes/hybrid forming):

A recently popular technique for boosting the catalytic performance of nanozymes involves the incorporation of several metals into a single lattice, resulting in changes in physicochemical and electronic properties of the multicomponent structure, thus a higher catalytic activity than single metal counterparts. For example, the addition of a few atomic Ir layers into the surface or Pd-cubes leads to the enhancement of catalytic efficiency up to 20 folds more than Pd-cubes and more than 400 folds of HRP as shown in Figure 4 [78].

Metal doping can introduce additional active sites, modify the electronic structure, and improve the stability of the nanomaterial [79]. In another example, Liu *et al*. reported that the peroxidase activity of cobalt-doped iron oxide NP enhanced up to 100-fold, regarding its H_2O_2 affinity compared to Fe_3O_4-NP [80].

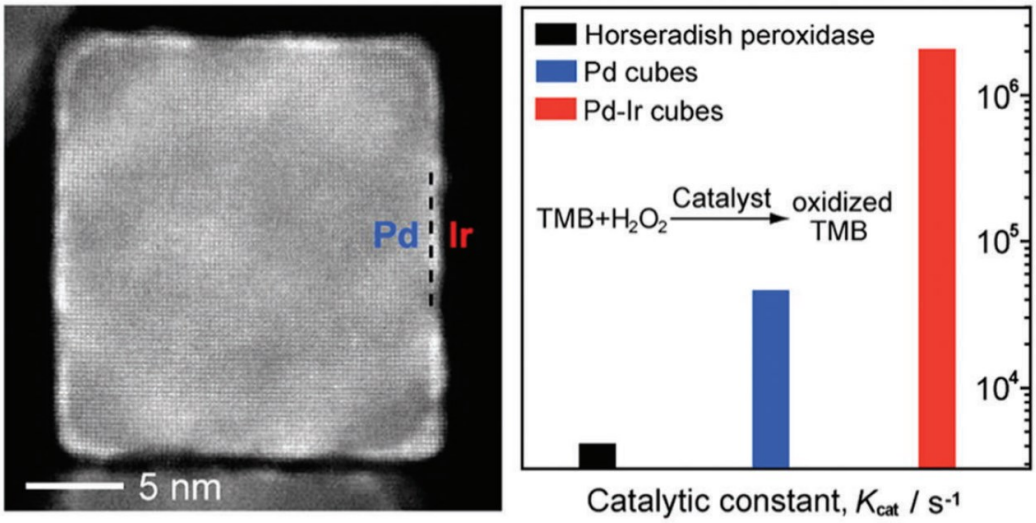

Figure 4. An efficient peroxidase-like activity of Pd-Ir cubes. Adopted from Xia et al. [78]*, copyright American Chemical Society 2015.*

Studies have shown that catalytic activity can be enhanced through the conjugation of different nanomaterials, resulting in a synergistic effect. For example, Pd-Pt-Fe_3O_4-NP demonstrates higher peroxidase-mimetic activity than individual nanoparticles [81]. Metal doping using nanometals such as MoS_2, CuO, or Pt nanoparticles has also demonstrated higher catalytic activity [82][83].

Additionally, nonmetal materials and natural enzymes can be used for higher catalytic activity, improved substrate selectivity, or modification of the nanozyme's susceptibility [70][84][85].

Doping with other metal ions can result in nanoparticles with multiple enzyme-like activities, which are summarized in Table 1 with enzymatic parameters and catalytic mechanisms, including the peroxidase-suggested mechanism of their catalytic activity and the peroxidase substrate.

Table 1. Different nanozymes from different classes, and their studied enzymatic activities, focusing on the peroxidase-like mechanisms and enzymatic parameters (K_M / V_{Max}), where K_M is known as Michaelis constant, which represents the affinity of nanozyme to the substrate and V_{Max} represent the maximum reaction velocity.

Nanozyme	Enzyme activity	Substrate	K_M (mM)	V_{Max} ($nM.S^{-1}$)	Peroxidase-like Mechanism	Ref.
Au/Ag	Peroxidase/ Oxidase/ SOD	TMB	0.396	14.1	Electron transfer reaction	[54]
FePt/Au	Peroxidase	TMB	0.445	246.7	Hydroxyl radical / Electron transfer	[86]
$CoFe_2O_4$	Peroxidase/ Oxidase/ Catalase	Different (K_m and V_{Max}) based on the size of nanoparticles.			Hydroxyl radical	[87]
$CuFe_2O_4$	Catalase/Peroxidase/ oxidase	H_2O_2	0.00118	82.3	Unclear	[88]
$Fe_2(MoO_4)_3$	Peroxidase	TMB	1.126	37.3	Hydroxyl radical	[89]
Au-Fe_3O_4	Peroxidase	H_2O_2	4.27	28.9		[90]
PtPd-Fe_3O_4	Peroxidase	TMB	0.079	93.6		[81]

6. Applications of Nanozymes

The investigation of numerous enzyme-like substances resulted in the integration of nanozymes in various bio-applications, as illustrated in Figure 5. Their distinct characteristics have made them suitable for applications such as anti-oxidation, biosensing, and bioimaging. Furthermore, more intricate in-vivo applications have been explored, including disease therapy, particularly tumor therapy, and anti-bacterial applications, among others. This subsection will detail the most prevalent bio-applications associated with nanozymes.

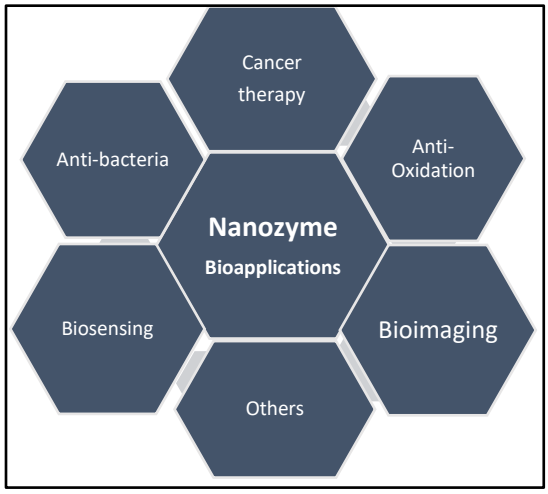

Figure 5. Illustration of different bio-applications of nanozymes.

6.1. Anti-oxidation: ROS are normally produced in human cells, but the excess generating and accumulation of ROS inside the cells cause harmful events. Nanozymes, which possess antioxidative properties such as low dose Ce-NP can scavenge the excess free radicals in the liver cells due to their SOD-like activity, preventing the cell from early apoptosis and DNA damage [91] in addition to its activity in protection against ischemic stroke [92]. Another example is MnO_2 nanozyme, which has been reported as a protector for the cell against physiological stressors such as superoxide radical $O_2^{\bullet -}$ by catalyzing radicals into water and molecular oxygen [93].

6.2. Cancer therapy: research continues always when it comes to cancer therapy, due to the unsatisfied results of chemotherapy and their harmful side effects, which makes enzyme-like mimetics a choice as toxic agents because of their ability to produce oxidative stress in an acidic medium like they can clear the free radicals in physiological pH. Therefore, nanozymes could result in apoptosis for cancer cells without harming the normal tissues around them, as the cancer cells possess acidic media in contrast to the normal cells where the medium is weak basic (physiological pH) [94]. Recently, chemo-dynamic therapy (CDT) has been widely used in cancer therapy, through Fenton-like reaction H_2O_2 converted to hydroxyl radical ($OH^{\bullet}$), which accumulated into cells leading to apoptosis [95]. Nitrogen-doped porous carbon nanosphere was reported by Yan *et al.* as a multifunctional enzyme-mimetic, it possesses POD-, oxidase-, catalase, and SOD-like activity, where it exhibits POD and oxidase in a slightly acidic microenvironment [15]. Furthermore, when it is combined with ferritin, the combination can selectively enter the lysosome stimulating production of more ROS, which increases the efficiency of the nanozyme therapy.

6.3. Antibacterial: Due to the increasing drug resistance of bacteria resulting from the excessive use of antibiotics, the development of an alternative treatment to overcome the challenges posed by bacterial infections has become imperative. Bacteria have the ability to create a biofilm that acts as an extracellular matrix barrier to protect them against antibiotic penetration [96]. Nanozymes such as Cu_2WS_4 nanocrystals [97], Ag/g-C_3N_4 hybrid [98] and silver ions-infused porphyrin (MOF) [99] exhibit a broad spectrum antibacterial activity owing to their inherent enzyme-like properties. For instance, Cu_2WS_4 nanocrystals show peroxidase-like and oxidase-like activity enabling them to eliminate both gram-positive and negative bacteria through excessive ROS production.

6.4. Biosensing: Many nanozymes have been utilized due to their enzyme-like activity in biological substrate detection such as blood glucose, uric acid, ROS, phosphatase, and others. For example, ultrasmall Au-nanoclusters are reported to be used as multifunctional protease biosensors for colorimetric detection due to their POD-like activity [100].

6.5. Bioimaging: Nanozymes have found extensive use in the detection of biological analytes in vitro and in vivo imaging, including live cells, organ imaging, and disease monitoring. For example, the ability of NiO nanozyme to mimic the activity of oxidase allows it to oxidize amplex-red, which is a weak florescent agent used as an indicator of cell viability, in physiological conditions. This characteristic makes it highly effective for intracellular imaging. [101].

7. High-entropy Nanomaterials

7.1. High entropy Nanomaterials (HEN) overview

High entropy nanomaterials (HENs) have recently gained attention in the field of catalysis due to their unique composition and structure. The high degree of structural disorder at the nanoscale in HENs can create an abundance of active sites for catalytic reactions, resulting in enhanced catalytic activity. These materials exhibit unique chemical stability and can be easily modified to optimize their catalytic properties, making them promising candidates for a wide range of catalytic applications. The synthesis of HENs with tailored compositions and structures is a complex process, often involving high-energy ball milling or other techniques. However, recent advances in materials science have made it possible to design and fabricate HENs with precise control over their composition and structure, opening up new possibilities for the development of innovative catalytic technologies. With their potential to significantly improve catalytic efficiency, HENs are expected to play an increasingly important role in the field of catalysis in the years to come. High-Entropy materials are composed of five or more principal elements with almost equal atomic fractions [102].

High entropy oxides (HEOs) are a novel type of high entropy nanoparticles (HENs) that have received considerable attention in recent years due to their distinctive features. HEOs are comprised of numerous metal cations that are arranged in a disordered manner within the lattice, resulting in a high degree of structural complexity. The disorder within HEOs is responsible for their unique characteristics, such as elevated surface area and improved catalytic activity. HEOs have been extensively investigated for their prospective utilization in various domains, such as catalysis, energy storage, and environmental remediation.

7.2. Core effects of high-entropy nanoparticles (HEN)

High-entropy materials are characterized by four main properties as illustrated in Figure 6. (a, b, c, and d), that describe and distinguish the nature of HEN. These four core effects will be explained in this section, in addition to the stabilization phase of HEO.

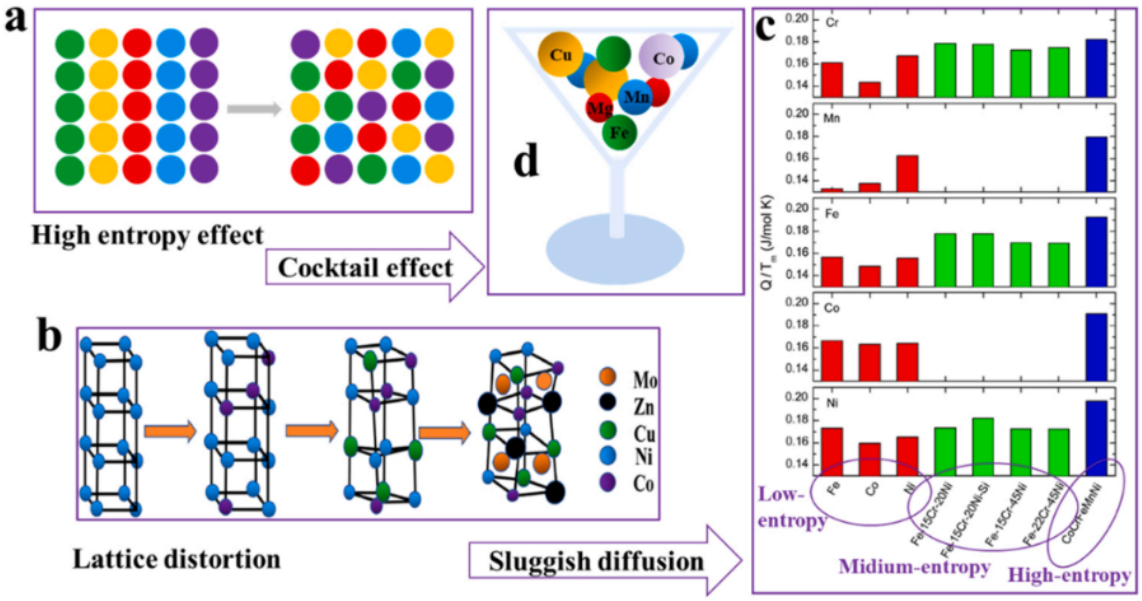

Figure 6. An illustration represents the core effects of HEN (a) High entropy effect: increase the compatibility between components to reduce the total free energy. (b) Lattice distortion: different molecular sizes between the principal elements. (c) Sluggish diffusion: higher diffusion activation energy due to the difference in the diffusion rate of elements. (d) the cocktail effect: describes the synergistic effect of multi-component material based on principle elements. (a,b) Copyright ELSEVIER 2020 and (c,d)Copyright Springer 2013.

The stabilization of the mixed elements in the solid solution is represented by Gibbs free energy law as shown in Scheme 7. HEN act as a single solid solution equally distributed in a crystal lattice [103].

$$\Delta G_{mix} = \Delta H_{mix} - T\Delta S_{mix} \qquad \textit{Scheme 6}$$

Where (G_{mix}) represents Gibbs free energy, (H_{mix}) is the Enthalpy of the mixture, (T) is the absolute temperature, and (S_{mix}) represents the Entropy of the mixture. From Scheme 7, Gibbs free energy decreases with the increase of Entropy of the Mixture, which in return provides a more stable Solid Solution mixture [104].

The Temperature, the number of elements, and the atomic fraction of elements in the composition influence the change in Entropy according to the following equation[105]:

$$\Delta Smix = -R \sum_{N}^{i=1} xi \, lnxi \qquad \textit{Scheme 7}$$

Where (R) represents the universal gas constant, (N) is the total number of elements and (xi) is the atomic fraction of each element. Based on Scheme 8, the maximum Entropy is achieved with an equal atomic fraction of each element with a high number of elements.

As shown in Figure 7. a. there is a direct correlation between the number of elements and the entropy ΔS_f, as the entropy increases with the increase of elements number.

Based on the classification of Murty and his colleagues for various alloy systems in Figure 7 (b), the High entropy alloys show $\Delta S_f \geq 1.5R$, while medium-entropy alloys present $R \geq \Delta S_f > 1.5R$ and low-entropy alloys $\Delta S_f < R$.

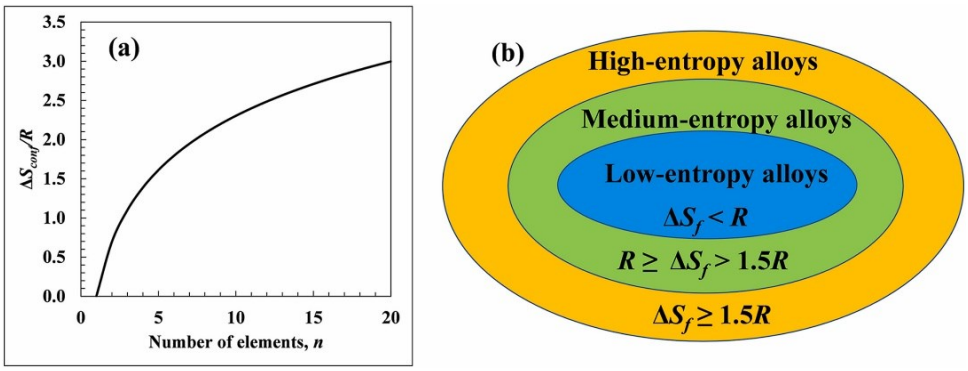

Figure 7. (a) The Relation between the entropy (ΔS_{conf}) and the number of elements in High-entropy metals. (b) The classification of alloys according to the entropy of the system. Adopted from Murty et. al. [106]

Phase stabilization is an important parameter for high-entropy material synthesis, which is influenced by the core effects of HEN such as the high-entropy effect, cocktail effect, sluggish effect, and lattice distortion effect. In this section, we will briefly describe each effect and explain its role in HEN stabilization and application [102,104,105,107,108].

First**, the High-Entropy effect** refers to the increased entropy of the material due to the presence of multiple cations. This effect can lead to a higher degree of disorder in the material, resulting in unique properties such as increased thermal stability and improved mechanical properties as shown in Figure 6 (a). The high-entropy effect has been demonstrated in several high-entropy oxide systems, including AlCoCrCuFeNiOx and MgCoNiCuZnOx [109–111]. Thus, the high entropy effect provides HEN with higher phase stability at very high temperatures.

Secondly, the **Sluggish effect** refers to the slow diffusion of ions within the material. The presence of multiple cations in HEN leads to an increased number of lattice sites, making it more difficult for ions to move around as shown in Figure 6 (c). As a result, high-entropy oxides tend to have a slower rate of phase transformation compared to conventional materials. This sluggish effect can be beneficial in certain applications, such as high-temperature thermal barrier coatings, where the material's stability is critical. Due to its dependence on different diffusion rates of different types of atoms in HEN, the change in chemical bonds, and potential energy, which leads to a lower diffusion rate, HEN displays a higher thermal and chemical stability than single-component nanomaterials [112].

Thirdly, **The Cocktail effect** as shown in Figure 6 (d), assures the effect of primary elements on the multi-component metals and provides unique features of HEN such as high strength, thermal stability, and catalytic activity due to the multiple cations present in the material [113]. This effect can result in high thermal stability, increased hardness, and improved chemical resistance. By combining different cations in high-entropy oxides, researchers can tailor the material's properties for specific applications, such as catalysis and energy storage.

Finally, **the lattice distortion** due to combining more than one element with different atomic sizes into the same lattice leads to the creation of many oxygen vacancies within the structure as shown in Figure 6 (b), which leads to lattice distortion or in other cases amorphous structures and the appearance of various mechanical, electrical, chemical and optical behaviors [112]. For example, high-entropy oxides have been shown to have enhanced photocatalytic properties due to their lattice distortion, which promotes the separation of photo-generated electrons and holes [114].

The combination of these characteristics has significant implications for the phase stabilization of high-entropy nanomaterials. The sluggish effect, for example, can prevent the material from undergoing phase transformation, resulting in a stable material that is suitable for high-temperature applications. The lattice distortion effect and the cocktail effect can be used to tailor the material's properties, such as increasing its catalytic activity or improving its chemical resistance. Finally, the high-entropy effect can result in a material with enhanced mechanical and thermal properties. Therefore, these four core effects sculptured the structural characteristics that influence the catalytic activity and different chemical, optical, thermal, and electrical properties of HEN [109].

Understanding these characteristics is critical for developing high-performance high-entropy materials for a wide range of applications.

7.3. Structures, Synthesis Methods, and Applications of HEN:

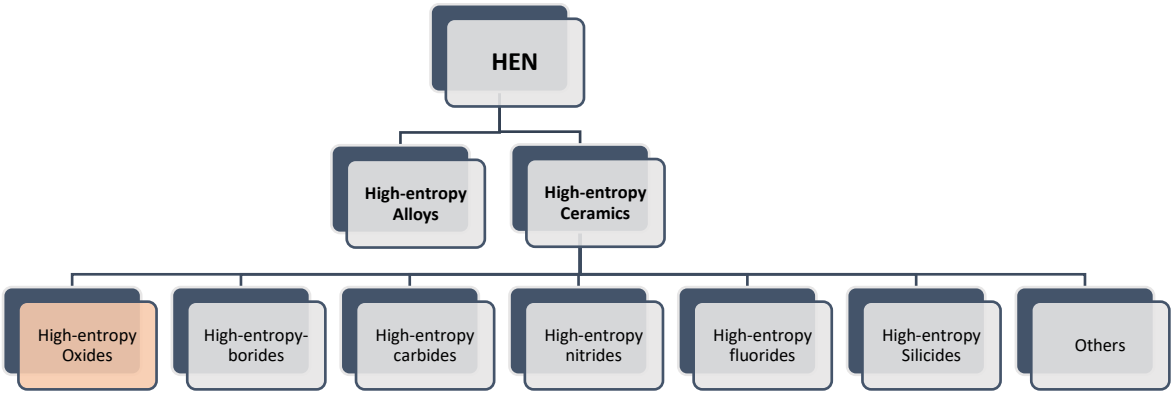

Scheme 9. A typical differentiation of high-entropy metals showing different classes of high-entropy ceramics.

The synthesis methods of HEN are determined according to the principle elements and the structure of HEN [104,115]. Scheme 9 shows the main classification of HEN into two categories high-entropy alloys (HEA) and high-entropy ceramics (HEC), each category characterized by different properties, and to keep the focus on the aim of the thesis, only HEC materials are mentioned in this section. High-entropy ceramics contain a wide range of classes according to the involved anion in the system such as high-entropy oxides, borides, carbides, and others. Recently, a huge attention to high-entropy oxides due to the involvement of oxygen anions within the structure, which plays a role in the catalytic action. For a better understanding of the tested material in this study high entropy oxide (HEO), Table 2 demonstrates some classes of HEC including HEO, with synthesis methods, available structures, and suggested applications.

Table 2. Different HECs with the relative method of synthesis, crystal structures, and applications in industrial and environmental fields.

HEC	Synthesis methods	Crystal structures	Suggested applications:	Ref.
High-entropy oxides(HEOs):	High energy ball milling, Solvothermal method, Sol-gel method, Solid state method, High-pressure Torsion, Mechanochemical method, Carbothermal shock, and others.	Fluorite, Rock-salt, Spinal structure, amorphous structure, and Perovskite.	CO- oxidation, desulfurization, Li-Sulphur batteries, Co_2 reduction, photocatalysis, and benzyl alcohol oxidation.	[116–121]
High-Entropy Carbides(HECs):	Sintering method, ball-milling method, Thermal reduction, and others.	Rock-salt structure (Cubic)	protective coatings.	[122,123]
High-Entropy Fluorides (HEF):		Perovskite structure.	electrocatalytic applications, laser industry.	[124–126]
High-Entropy Phosphates ($HEPO_4$):	coprecipitation method.	Monazite-type.	barrier coating materials and Catalytic activity.	[127,128]
high-entropy silicides (HESis):	mechanical milling and spark plasma sintering.	Hexagonal structure.	Coating and integrated circuit electrode films.	[129,130]

Aim of thesis

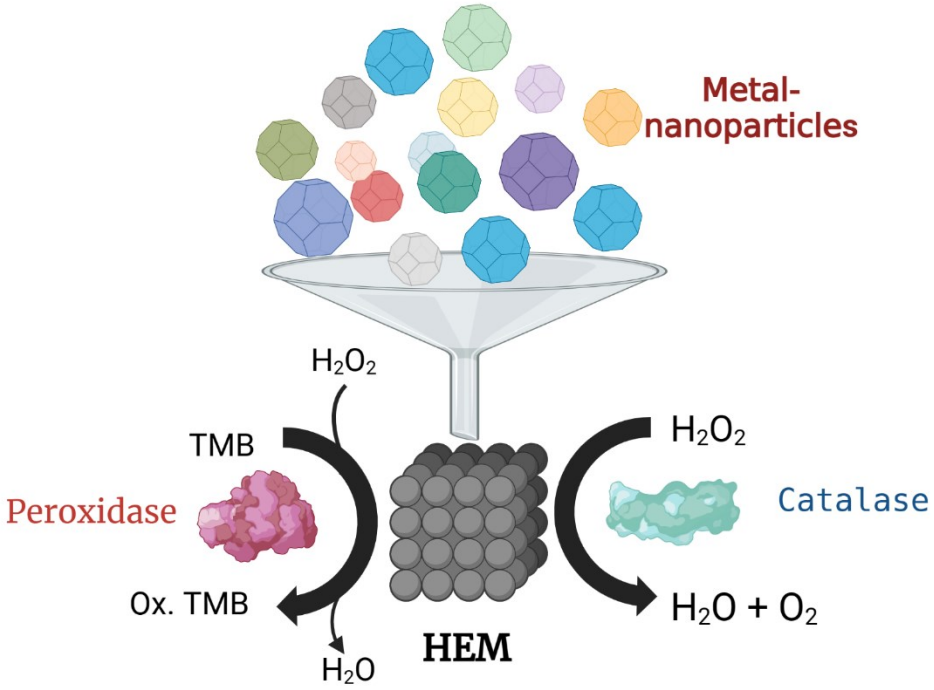

Figure 8. Illustration scheme demonstrating the aim of the thesis, where different metal-nanoparticles forming high-entropy material (HEM), shows multienzyme-like activity (Peroxidase and catalase).

Since the discovery of the intrinsic peroxidase-like activity of Fe_3O_4-NP, huge attention has been paid to seek for new nanomaterials with enzyme-like activity. As mentioned previously, incorporating different metals into the same lattice can improve the catalytic performance of nanomaterials or even offer new enzymatic activities. Those researches, however, have been restricted to bimetallic or trimetallic nanoparticles. A previous study in our group showed that high entropy nanomaterials also possess peroxidase-like activity, depending on metal compositions. In this study, we will focus on investigating mechanisms of peroxidase-like activity of a selected high entropy material $(FeCr)(CuFeMn)_2O_4$ as well as enzymatic parameters according to Michaelis-Menten kinetics, in comparison with the reference Fe_3O_4 nanoparticle. In addition, another enzymatic activity of this material (catalase) will be also determined.

II. Experimental section

1. Materials and instruments

1.1. Chemical substances

High-entropy nanoparticle $(FeCr)(CuFeMn)_2O_4$ with a particle size of 374 ± 8 nm, and Fe_3O_4-NP with a particle size of 270 ± 7 nm were produced by ball-milling and kindly provided by our collaborator Dr. Ben Breitung, Institute of Nanotechnology, Karlsruhe Institute of Technology (KIT), Germany.

3,3',5,5' tetramethylbenzidine (TMB), Sodium acetate (Na ac.), Acetic acid, Peroxidase from Horseradish (lyophilized powder) with a concentration of 150 U/mg, Terephthalic acid, Europium chloride (Eu-Cl_3), Tetracycline hydrochloride, MOPS sodium salt, and native catalase enzyme extracted from bovine liver (lyophilized powder) with concentration 2000-5000 U/mg, and 1,4 Benzoquinone (p-BQ) purchased from Sigma Aldrich chemicals. Dimethyl sulfoxide (DMSO) and Sodium hydroxide were purchased from Carl Roth company. Reduced Cytochrome C purchased from ABCAM.

1.2. Instruments

UV-vis Spectrophotometer from "Bio-Tek Instruments" Reference: EPOCH2NSC, with serial number 21031519. UV- Fluorescence Spectrophotometer microplate reader from TECAN model: infinite M200 PRO. Millipore Milli Q Ref A+ from MERCK for water purification.

Software for enzymatic analysis and graphs: Origin Pro 2023 learning Edition from OriginLab Corporation. Microsoft Excel version MS 365 from Microsoft.

2. Methods

2.1. Colorimetric assay using Michaelis-Menten kinetics for HEN $(FeCr)(FeCuCr)_2O_4$, Fe_3O_4 NP, and HRP

Firstly, HEN suspension (80 µg/ml) was prepared by diluting from 100 µL stock suspension (2mg/mL) with 1150 µL of miliQ-H2O. To eliminate any contamination left over during synthesis, the suspension was washed by centrifugation at 13000g, then the supernatant was taken out and nanoparticles were refilled with fresh milliQ-H2O.

In this experiment, the catalytic activity of HEN, Fe_3O_4 NP, and HRP on the substrate TMB in presence of H_2O_2 at a fixed concentration (500 mM), which was the concentration used in the study performed by Gao *et al.* [8]. A set of different concentrations of TMB (100 µM to 1500 µM) was prepared from a stock solution.

To investigate Michaelis-Menten kinetics of HENs, a peroxidase assay was carried out as followed: 100 µL of HEN suspension (80 µg/mL) was added in a quartz cuvette, followed by 78,4 µL of TMB solution in NaAC pH 4 and 21.6 µL of H_2O_2 solution, respectively. The concentration of TMB was varied from 100 µM to 1500 µM and the H_2O_2 concentration was 500 mM. The absorbance was measured at 650nm every minute for 15 minutes at RT. The measurement was repeated with 3 replicates.

The absorbance values were collected to calculate the mean values and standard deviation, in addition to calculating the slope of the first 5 minutes from the generated curve to represent the change in absorbance (ΔA). As referred to in Beer-lambert equation in Scheme 10, the initial velocity of the reaction (V_0) was calculated by the equation $\mathbf{v}_0 = \Delta A/(\varepsilon.\iota)$ ($M.Sec^{-1}$), where (ε) of the substrate TMB = 39.000 M^{-1}/cm^{-1}.

From the gathered data, Michaelis-Menten plot was generated, where the x-axis represents [S] the substrate concentration of TMB in (µM) while the y-axis represents the calculated initial velocity (V_0) in ($M.Sec^{-1}$).

For a further representation of the data, Lineweaver-Burk plot was also generated, which represents the reciprocal values of initial velocity ($1/V_0$) and substrate concentration 1/[S].

From the generated graphs, values of the maximum velocity of the catalytic reaction (V_{Max}) and the affinity of HEN to the substrate, referred to as Michaelis constant (K_M), were calculated to be compared later with the values of Fe_3O_4-NP and HRP.

Kinetic parameters of Fe_3O_4-NP and HRP were investigated according to a similar procedure to HEN. In the case of HRP, the concentration of HRP was 10 ng/ml and H_2O_2 was 17.6 mM.

Michaelis-Menten plot and Lineweaver Burk plot were generated. Finally, the affinity to TMB (K_M) of $(FeCr)(FeCuCr)_2O_4$, Fe_3O_4 NP, and HRP and the maximum velocity (V_{Max}) were calculated and compared with other data as shown in Table 3.

2.2. Data analysis (Michaelis-Menten enzymatic kinetics)

The principle of the experiment is based on the colorimetric detection of the oxidized product, which is produced through the reaction between peroxidase substrate and hydrogen peroxide, as shown in the following chemical equation in Scheme 10:

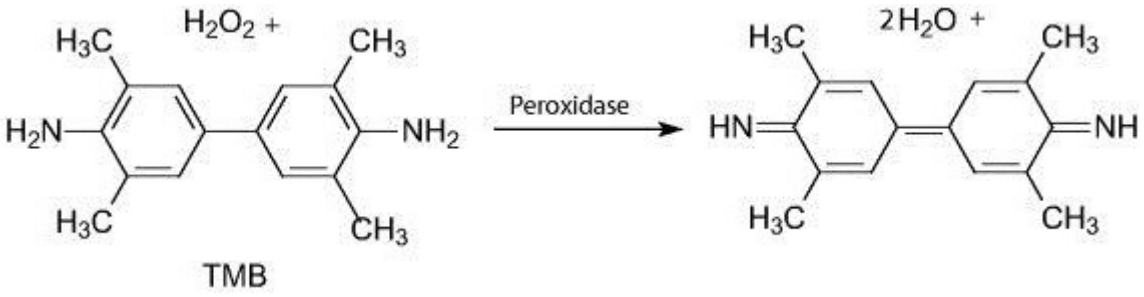

$$TMB + H_2O_2 \xrightarrow{HEN(POD-like\ nanozyme)} Ox.\ TMB + 2H_2O$$ *Scheme 10*

In Scheme 10, TMB represents the peroxidase substrate, high-entropy nanoparticles (HEN) are the nanozyme, that catalyzes the peroxidase-like reaction, and H_2O_2 is the second substrate, which acts as an oxidizing agent. The Michaelis-Menten kinetics was performed by varying the concentration of TMB (100 µM to 1500 µM) and fixed H_2O_2 concentration of 500 nm. The assay was carried out as described in section 2.2.

The colorimetric detection of a produced ox. TMP is based on measuring the absorbance (A) kinetically in 15 minutes, using a UV-vis Spectrophotometry device at wavelength 650 nm.

To obtain Michaelis-Menten parameters, the Beer-Lambert law was used to calculate the absorbance (A) of oxidized peroxidase substrate according to the equation in Scheme 11:

$$A = \varepsilon . \iota . c \qquad \textit{Scheme 11}$$

In the equation, (A) represents the absorbance measured by UV-vis spectrophotometry, (Ɛ) is the extension coefficient/molar absorption coefficient of the substrate (M^{-1}/cm^{-1}), (ι) represents the length of the light path in (cm), and (c) is the molar concentration of substrate in (M). The change in absorbance of the product in time appears in Figure 9 (a). To measure the initial velocity of the reaction (V_0) to be plotted in the Michaelis-Menten graph as in Figure 9 (b), we measure the change of concentration in time via the absorbance measurement, which is calculated from the slope of the produced curve of absorption, must be calculated as in Scheme 12:

$$Vo = \Delta c = \frac{\Delta A}{\varepsilon . \iota} \ (M.Min^{-1}) \qquad \textit{Scheme 12}$$

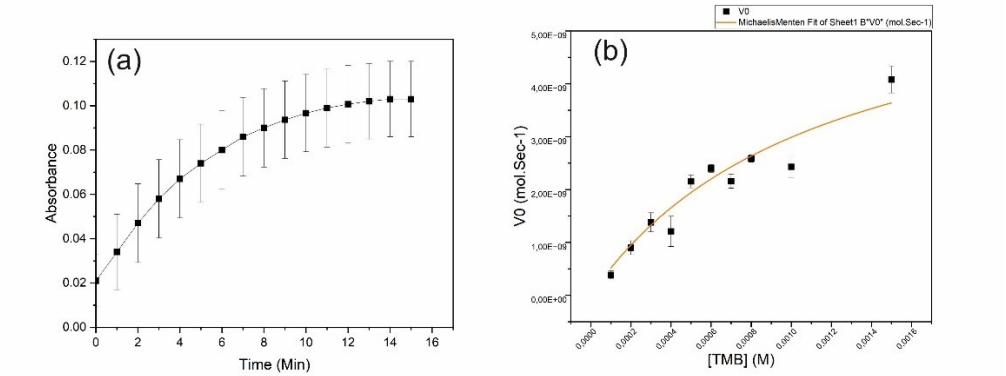

Figure 9. (a) A graph showing the change in absorbance (A) in time (T). (b) The change of reaction velocity in different substrate concentrations.

Michaelis-Menten kinetics is commonly used to investigate the catalytic activity of an enzyme regarding its affinity to the substrate (K_M) and the maximum velocity of the catalytic reaction (V_{Max}). The Michaelis-Menten equation in Scheme 13 describes the dependence of the conversion rate of the enzyme on the substrate concentration and therefore can predict the rate of an ongoing reaction.

$$\upsilon = \frac{Vmax\ .[S]}{Km+[S]} \qquad \textit{Scheme 83}$$

From Michaelis-Menten equation [S] represent the substrate equation and the Michaelis constant (K_M) is equal to the concentration of substrate when the velocity of the reaction is half of the maximum velocity of the catalytic reaction ($v = \frac{1}{2} Vmax$), therefore (K_M) calculated with units of Molarity (M).

In addition to Michaelis-Menten kinetics, the Lineweaver Burk plot is performed as an additional representation of enzymatic activity, as the following equation in Scheme 14:

$$\frac{1}{Vo} = \frac{Km}{Vmax.[S]} + \frac{1}{Vmax}$$ *Scheme 9*

Lineweaver Burk graph is generated by plotting the reciprocal of calculated velocity (V) versus the reciprocal of substrate concentration [S], therefore it is referred to as (a double reciprocal Burk plot). Due to the similarity of the straight line equation $\boldsymbol{(Y = m.x + C)}$, where the y-axis (Y) would be represented by $1/V_0$, the x-axis equals 1/[S], and (m) represents the slope of the line on the graph, that equals to (K_M/V_{Max}), and the intercept on the y axis (C) represents $1/V_{Max}$.

2.3. Investigating the peroxidase-like activity mechanism of HEN

The mechanism of peroxidase-like activity (as mentioned in the mechanism section from the introduction) can be the production of free radicals such as hydroxyl radical $OH^{\bullet}$ or Superoxide anion radical [O_2^-] through Fenton-like reaction or by electron transfer process involvement. It depends on the chemical structure, charges of cations, and chemical properties of the nanozyme [52,53,55,56].

2.3.1. Detection of hydroxyl radical ($OH^{\bullet}$) production

To prepare the terephthalic acid (hydroxyl radical scavenger) for detection, sodium terephthalate (NaTa) needed to be prepared by adding 10.4 mg of TA to a solution of 100 ml of sodium hydroxide NaOH, which was previously prepared by dissolving 6,3 mg of NaOH in 100 ml of MilliQ-H_2O. The prepared concentration of Sodium terephthalate NaTA to show the scavenging effect to $OH^{\bullet}$ free radical is 0.625 mM.

After preparing NaTa, three different concentrations of HEN were also prepared to detect the effect of concentration on $OH^{\bullet}$ production (20, 40, and 80 µg/ml). 24 µL of HEN suspension was added to an Eppendorf, followed by 200 µL of 0.625 mM sodium terephthalate, 120 µL of 1M NaAc, and 48 µL of 6.25 M H_2O_2 solution. The mixture was mixed and incubated for 8 hours at RT in a dark place. A negative control solution was prepared to contain NaTa, H_2O_2, and H_2O without HEN and incubated in the same conditions.

After incubation, the mixture was centrifugated at 13000g for 5 minutes. Then 200 µL of supernatant was transferred into a well and measured fluorescent intensity (excitation 315nm, emission 425 nm). The experiment was done with 3 replicates and in comparison with

the negative control. For the measurement of fluorescence emission, a UV- fluorescence Spectrophotometer was used to read the spectrum from 300-500 nm wavelength. Finally, the collected data were gathered and after calculating the mean value was generated for results visualization.

2.3.2. Detection of superoxide radical (O_2^-) production

A solution of 5 mM 1,4 Benzoquinone (p-BQ) in dimethyl sulfoxide (DMSO) was prepared, three concentrations of solution (40, 80, and 60 µg/ml) HEN was prepared as mentioned previously, 100 µL of HEN suspension (80 µg/mL) was added in a well, followed by 78.4 µL of TMB solution and 21.6 µL of H_2O_2 solution. Then 50 µL of 5 mM p-BQ solution in DMSO was added and the absorbance was measured every minute for 15 mins at 650 nm.

The experiment was repeated with 3 replicates. Results were presented as mean value and standard deviation.

iii. 2.3.3. Electron transfer process

In this experiment, Reduced Cytochrome C was used to detect if the electron transfer was included in the catalysis reaction in presence of HEN as a catalyst.

It is well documented that Cytochrome C in the reduced form shows two peaks at 520 nm and 550 nm. On the contrary, the oxidized Cytochrome C after losing electrons will show the disappearance of those two peaks and a newly developed peak will be seen at 530 nm [131].

Procedure: 350 µL of HEN suspension (80 µg/mL) was mixed with 140 µL of 1M NaAc, 45 µL of reduced cytochrome C, and 164 µL of milliQ-H2O. The mixture was incubated for 90 minutes in a dark place, then centrifugated at 13000g for 5 minutes. Subsequently, 200 µL of supernatant was added to a 96-well plate and the UV spectrum was scanned from 400nm to 600nm. A control sample without HEN was prepared at the same condition for comparison.

2.4. Catalase-like activity detection of HEN

To conduct the catalase assay, several solutions were prepared as follows:

10 mM MOPS buffer: 0.693 g of MOPS sodium salt was dissolved in 100 mL MilliQ-H_2O. pH was adjusted to 7.4 by glacial acetic acid, then the solution was filled up to 300 mL. The Prepared solution was kept in a dark place at RT.

Europium tetracycline (EuTc) solution was prepared by mixing 5 ml of EuCl3 solution (23 mg $EuCl_3$ in 50 ml MOPS buffer) with 5 ml of tetracycline chloride (50.5 mg tetracycline-HCl in 50 MOPS buffer), then filled with 40 ml MOPS buffer to obtain 50 ml of EuTc solution.

Catalase assay: In a 96-well plate, 50 µL of EuTc solution, 20 µL of 750 mM H_2O_2, and 165 µL of MOPS buffer were added, then the mixture was incubated for 20 minutes. After that, 50 µL of HEN was added and the fluorescent intensity (excitation 405 nm, emission 620 nm) was subsequently measured every 2 minutes for 20 minutes. Negative control (replacing HEN with

milliQ-H_2O) and positive control (replacing HEN with a solution of 0.1 mg/mL native catalase) were also prepared for comparison. The catalase activity was presented as mean decreased fluorescent intensity (%) with standard deviation obtained from 3 replicates.

III. Results

Based on the aim of the thesis the peroxidase- and catalase-like activity of tested HEN were detected in addition to the determination of a peroxidase-like reaction mechanism.

1. Michaelis-Menten kinetics of HEN regarding peroxidase-like activity

Investigation of Michaelis-Menten kinetics of HEN was carried out by varying TMB concentration from 100 to 1500 µM and a fixed H_2O_2 concentration of 500 mM in presence of 40 µg/mL of HEN.

The velocity was calculated by measuring the absorbance of oxidized TMB in Scheme 12, then a graph of TMB concentration versus velocity was plotted as shown in Figure 10 (a).

Lineweaver-Burk line was obtained (R^2 = 0.987) by plotting the reciprocal concentration of TMB against reciprocal velocity in Figure 10 (b). The graph was fitted into Michaelis-Menten kinetics mode in Origin Pro (version 2023), and enzymatic kinetic parameters were calculated with K_m = 0.507 mM, V_{Max}= 2.97E^{-08} M.Sec^{-1}.

Using the same procedure, Michaelis-Mente kinetics of 40 µg/ml of Fe_3O_4 NP was carried out in the same reaction conditions and substrate concentrations, in presence of 500 mM H_2O_2.

The Michaelis-Menten graph was plotted as shown in Figure 10 (a), in addition to the Lineweaver-Burk plot in Figure 10 (b) with (R^2 = 0.98), the graph was fitted into Michaelis-Menten kinetics mode in Origin Pro (version 2023), and enzymatic kinetic parameters were calculated with K_m = 0.54 mM, V_{Max}= 8.28E^{-09} M.Sec^{-1}.

Finally, for better comparison, the peroxidase activity of 10 ng/ml horseradish peroxidase in the same range of TMB concentration (100 – 1500 µM) was measured at the same reaction condition (at room temperature in pH = 4). Due to the higher sensitivity of HRP to H_2O_2, a much lower concentration was used (17.6 mM). The same measurement procedure was performed and data collected were used to generate the Michaelis-Menten plot and Lineweaver-Burk as shown in Figure 10. The maximum velocity of HRP catalytic reaction (V_{Max}) was calculated as V_{Max} = 3.90E^{-8} M.Sec^{-1}, while the affinity of HRP to (TMB) as peroxidase substrate K_M = 1.32 mM.

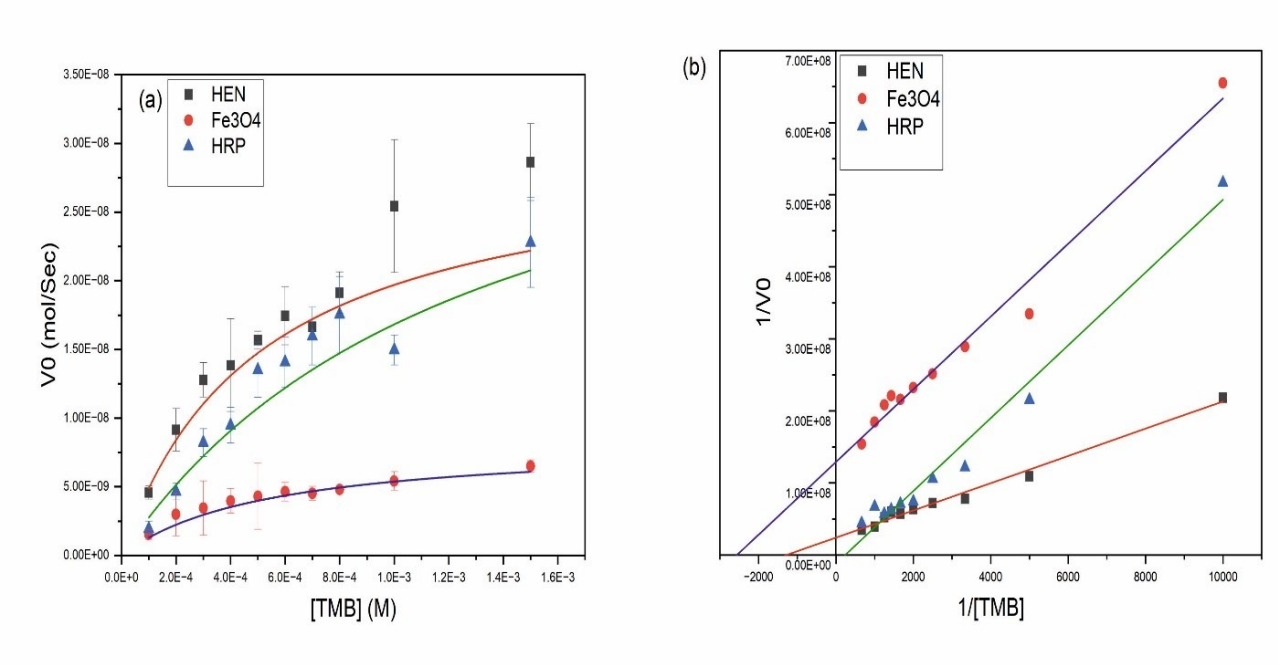

Figure 10. (a) Michaelis-Menten graph represents the enzymatic relation between the velocity of the reaction of (HEN, Fe_eO_4-NP, and HRP) and the concentration of substrate TMB, where the red line represents HEN activity, the green line shows HRP activity and the blue line represents Fe_3O_4NP activity. (b) Lineweaver-Burk plot shows a straight line with (R^2= 0.987, 0.981, 0.978) for HEN, Fe_eO_4-NP, and HRP respectively, representing the double reciprocal of the velocity and TMB concentration. (V_0) represents the reaction velocity and [TMB] is the concentration of TMB. Values represent the mean ± standard deviation of n=3 replicates.

In the following Table 3, the maximum catalytic reaction velocity V_{Max} and the affinity towards substrate (Michaelis constant K_M) for HEN, Fe_3O_4-NP, and HRP were represented.

Table 3. A demonstration of the maximum velocity, affinity to the substrate, R2 of Lineweaver-Burk plot, and H2O2 concentration for HEN, Fe_3O_4-NP, and HRP enzymatic activity.

	Substrate	Concentration of H_2O_2	R^2	Km(mM)	Vmax (M.S-1)
HEN 40 µg/ml	TMB	500 mM	0.987	0.507	2.97E-08
Fe3O4 40 µg/ml	TMB	500 mM	0.981	0.54	8.28E-09
HRP 10ng/ml	TMB	16.7 mM	0.978	1.32	3.90E-08

As shown in the previous Table 3, Km of HEN has the lowest value of 0.507 mM, which indicates the higher affinity of HEN towards TMB as substrate more than Fe_3O_4-NP which equals 0.540 mM, and HRP that equals 1.320 mM. Although the maximum velocity of enzymatic reaction belongs to HRP that means the velocity of HRP catalytic reaction is 1.31 higher than HEN catalytic reaction.

2. Hydroxyl radical production

It has been reported that hydroxyl radicals are involved in the peroxidase-like activity of nanozyme. The detection of hydroxyl radicals is based on the reaction of terephthalic acid with OHs radical to form hydroxyl terephthalate which has strong fluorescent signal. As can be seen in Figure 11, a peak was absent at 425 nm at any tested concentration, indicating no hydroxyl radical was produced.

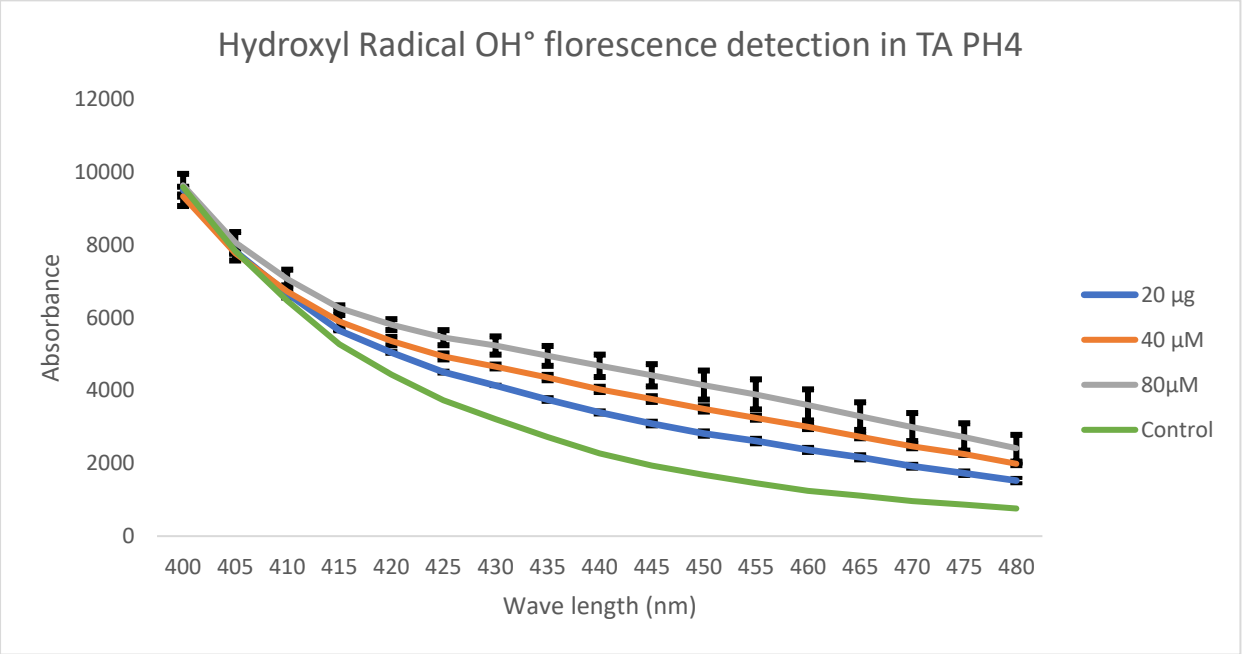

Figure 11. Fluorescence spectrum from 400 – 480 nm for 20, 40, and 80 µg/ml HEN, 1 M of H_2O_2, and 0.625 mM sodium terephthalate compared with control (absence of HEN) shows no difference in spectrum between all tested concentrations and control, which indicates the absence of hydroxyl radical. Values represent the mean ± standard deviation of n=3 replicates.

This result interprets the absence of $OH^{\bullet}$ production, therefore hydroxyl radical can not explain the mechanism of the peroxidase-like reaction of HEN.

3. Superoxide radical production

Using a UV-vis spectrophotometer, the reaction rate for three HEN concentrations was measured every 60 seconds for 15 minutes at wavelength 650 nm to detect the oxidized TMB production in the presence and absence of p-BQ. The data was gathered, and the average value for three replicates of each concentration was calculated, in addition to the standard deviation and slope for the first 5 minutes.

The reaction rate of HEN with TMB in the presence or absence of p-BQ was compared and reported in Figure 12. The negative control was done as well to show the effect in absence of HEN on the reaction.

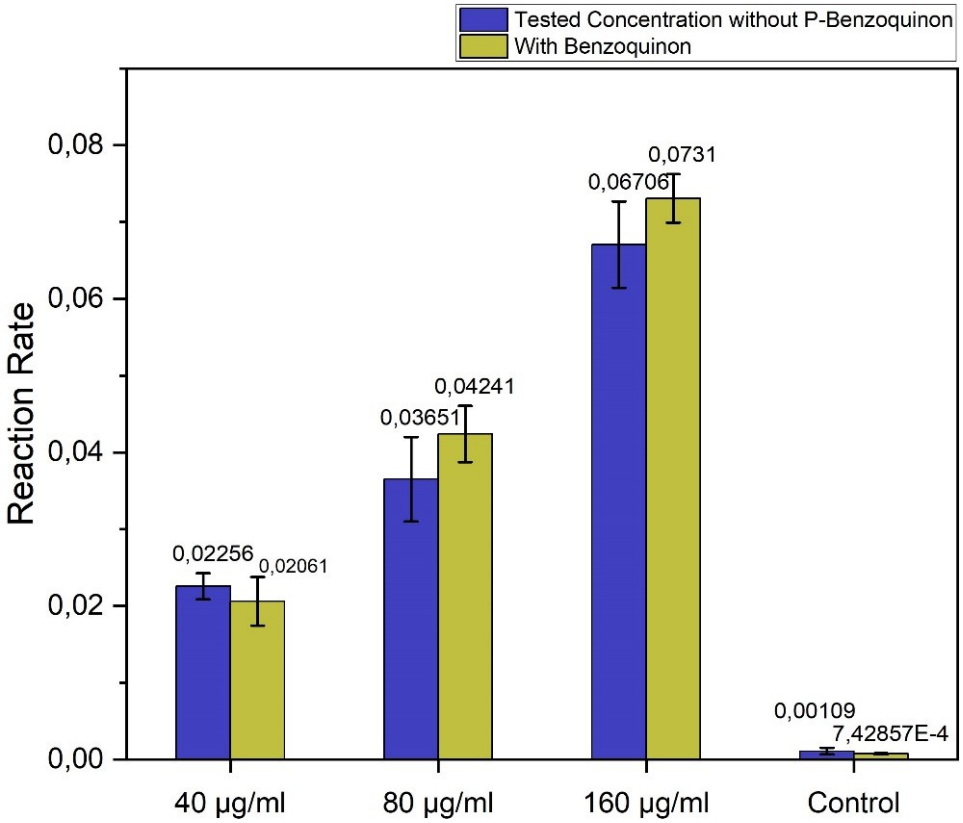

Figure 12. The reaction rate of 40, 80, and 160 µg/ml of HEN in the presence (green) and absence (blue) of p-BQ with TMB in presence of H_2O_2, showing a negative control (without HEN) show the effect on the reaction and exclude any interference of p-BQ to the reaction rate. Values represent the mean ± standard deviation of n=3 replicates.

As can be seen, there was no significant change in reaction rate in the presence and absence of p-BQ, (P-values of 0.483, 0.275, 0.256 were calculated for concentrations 40, 80, and 160 µg/ml respectively), which means that the presence of p-BQ does not affect the reaction due to the absence of superoxide radical. Therefore $O_2^{\bullet-}$ is not responsible for the catalytic mechanism.

4. Electron transfer process involvement.

The determination of the electron transfer process is based on the conversion of reduced Cytochrome C to its oxidized form as shown in Figure 13. Cytochrome C in the reduced form will show two peaks at 520 nm and 550 nm. On contrary, the oxidized Cytochrome C after losing electrons will show the disappearance of those two peaks and a newly developed peak will be seen at 530 nm. The control was prepared as well to compare the change in the spectrum by adding the same amount of Cytochrome C, Buffer, and H_2O without HEN.

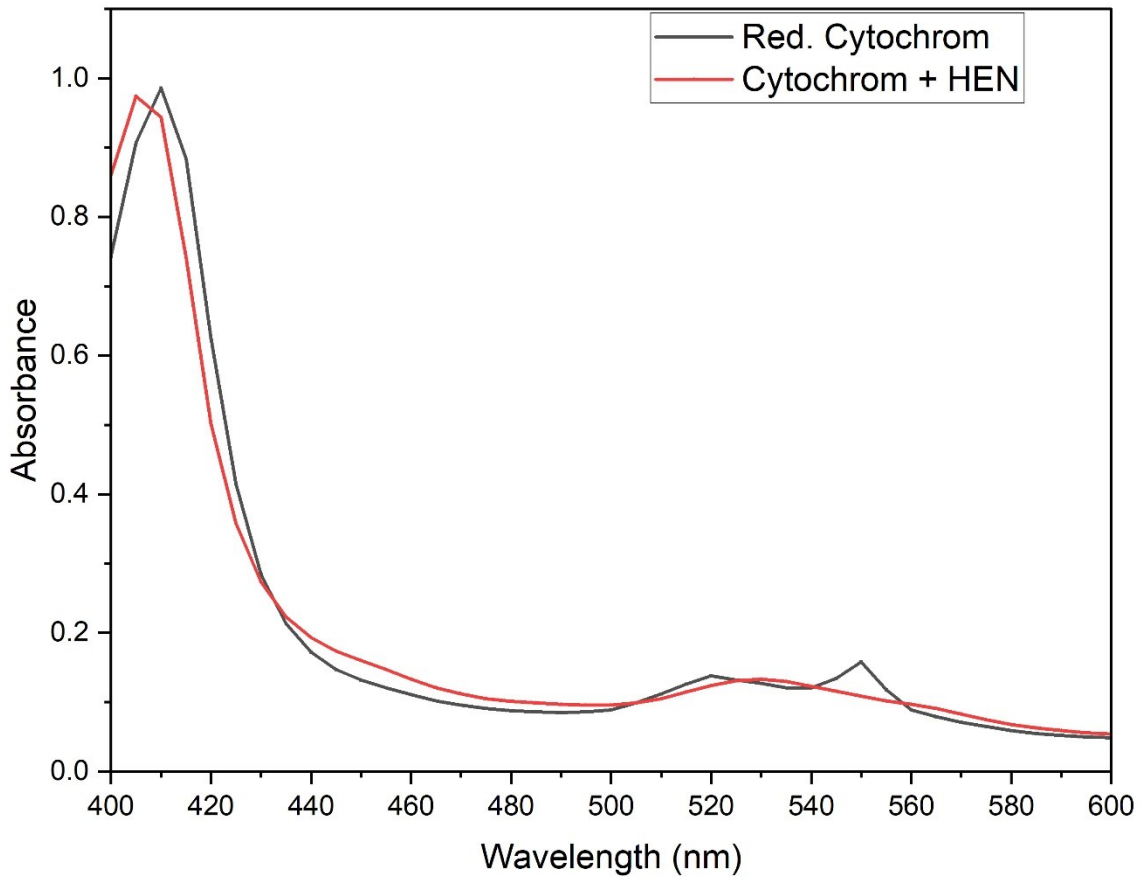

Figure 13. shows a Spectrophotometric analysis of Cytochrome C involved in the electron transfer process of the Peroxidase reaction, as the Black line shows reduced Cytochrome C with two peaks at 520 and 550 nm, on the other hand, the red line shows only one Peak at 530 nm.

The spectrum shows in the presence of HEN an appearance of a peak at 530 nm and vanishing the two peaks at 520 and 550 nm, which indicates the oxidation of Cytochrome C as a result of losing an electron during the reaction, in comparison to the black line (reduced cytochrome) in absence of HEN the two peaks at 520 and 550 nm.

That confirms the involvement of the electron transfer process in the peroxidase-like reaction of HEN and explains its mechanism of activity.

5. Catalase-like activity of HEN

A fluorescence spectrophotometer was used to analyze the change in fluorescence intensity of EuTc after the catalase reaction, as a result of the decomposition of the EuTc-HP complex.

The reduction in the fluorescent intensity was reported and values were gathered, average of three trials for each concentration was calculated, standard deviation and the percentage of fluorescence reduction for each concentration and control were visualized in Figure 14(a).

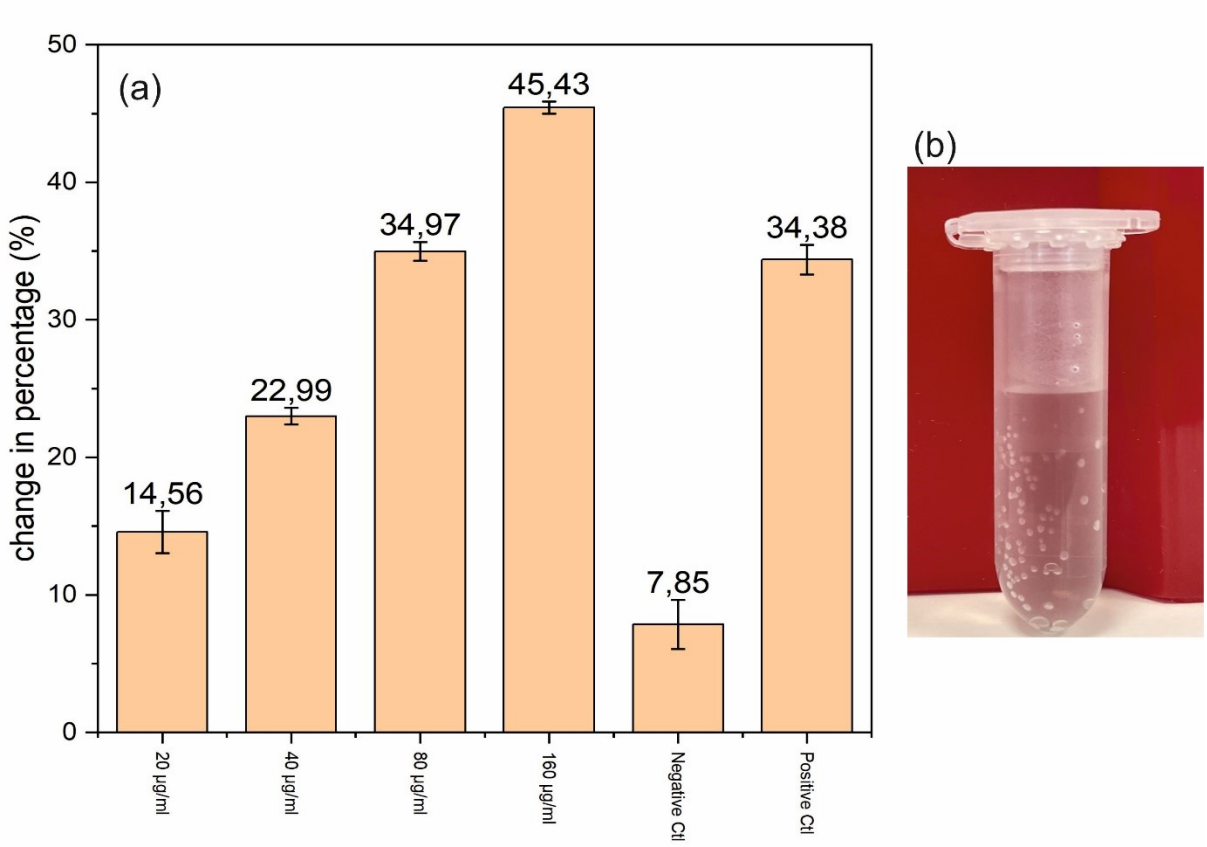

Figure 14. (a) The graph shows the percentage of fluorescence reduction over time for four concentrations of HEN (20, 40, 80, and 160 µg/ml) in comparison to negative and positive (with native catalase enzyme) control. Values represent the mean ± standard deviation of n=3 replicates. (b) The catalase-like activity of HEN appears in the production of oxygen bubbles as a result of H_2O_2 decomposition.

For better interpretation, decreased fluorescent intensity in percentage was used. Graph 14(a) shows there was a decomposition of H_2O_2 in the mixture, determined by the decrease of fluorescent intensity over time. In addition, catalase-like activity increased with the increase in HEN concentration. As can be seen in Figure 14, a HEN concentration of 80 µg/ml showed a comparable performance as native catalase. The negative control also showed a reduction of fluorescent intensity which may be attributed to the auto-decomposition of H_2O_2 over time. However, this decrease was much more pronounced in presence of HEN.

IV. Discussion

While many papers reported the electro-, photo- and thermo-catalysis activities, the focus of this thesis will be on the multienzyme activity of high-entropy oxide and its catalytic mechanism.

The enzymatic kinetics of peroxidase-like activity of HEN was determined according to Michaelis-Menten kinetics and subsequently compared the results with Fe_3O_4-NP and HRP results as references of peroxidase activity. For peroxidase-like activity determination, TMB had been used as a peroxidase substrate with a set range of concentration (100-1500 µM) in presence of H_2O_2 at 500 mM concentration, which is the same H_2O_2 concentration in the previous study by Gao *et al*. 2007 [8]. It turned out that, HEN showed a higher affinity to substrate 2.6 folds more than HRP, as Michaelis constant Km of HEN, Fe_3O_4-NP, and HRP were 0.507, 0.54, and 1.32 mM, respectively. On the other hand, HEN showed a faster catalytic reaction rate than Fe_3O_4-NP 3.6 folds but slower than HRP, where V_{Max} of HEN, Fe_3O_4-NP, and HRP was $2.97E^{-8}$, $8.28E^{-9}$, and $3.9E^{-8}$ $M.Sec^{-1}$, respectively.

Substrate Affinity K_M: HEN > Fe_3O_4-NP > HRP (HEN has 2.6 times Higher Affinity than HRP).

Reaction velocity V_{Max}: HRP > HEN > Fe_3O_4-NP (HEN reacts 3.6 times faster than Fe_3O_4-NP).

However, the results from the study done by Gao *et al*. 2007 showed a better affinity for Fe_3O_4-NP to TMB with K_m= 0.098 mM and the affinity of HRP K_m= 0.434 mM, in addition to the catalytic reaction velocity V_{Max} = 3.44 E^{-8} and 10.00 E^{-8} for Fe_3O_4NP and HRP respectively. These differences were shown due to the difference in conditions of reaction, as the temperature of reaction at Gao's study was 40 °C and the particle size of Fe_3O_4NP was 30 nm, which showed the maximum activity of nanozyme.

Peroxidase-like mimetics exhibit varied catalytic activities, which include free radical production and participation in the electron transfer process. The Fenton-like reaction is a well-known and extensively studied mechanism of peroxidase and peroxidase-like reactions that generates hydroxyl radicals. In this reaction, hydrogen peroxide is attracted to the surface of nanozyme, leading to the cleavage of the O-O bond, producing $OH^{\bullet}$, which subsequently oxidizes the peroxidase substrate into an oxidized colored product. To detect the production of $OH^{\bullet}$, a hydroxyl radical scavenger is necessary, which can be detected or measured using fluorescence techniques. The hydroxyl radical scavenger TA is regarded as effective due to its high affinity to $OH^{\bullet}$, and it can detect as low as 2 nM of $OH^{\bullet}$ [132]. The equation presented in Scheme 15 shows that TA reacts with $OH^{\bullet}$ to form a fluorescent product called 2-hydroxy-terephthalic acid (hTA).

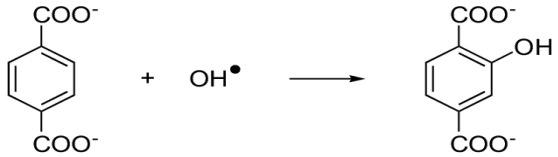

Scheme 105

The result showed no difference in fluorescence spectrum at the end of the reaction between samples in the presence and absence of HEN. This result indicates that hydroxyl radical is not responsible for the catalytic activity mechanism of HEN.

During the peroxidase-like reaction of HEN with the substrate, another free radical that may be produced is the superoxide radical [$O2^{\bullet-}$], which promotes the oxidation of the peroxidase substrate to yield the oxidized colored product. The detection of superoxide radical [$O2^{\bullet-}$] production in the peroxidase-like reaction follows a similar concept to detecting hydroxyl radical $OH^{\bullet}$. A superoxide scavenger, 1,4-benzoquinone (p-BQ), is used to detect the production of superoxide radical [$O2^{\bullet-}$] from the catalytic reaction of nanozyme. P-BQ reacts with [$O2^{\bullet-}$] expected to be produced, resulting in the formation of hydroquinone (H2Q), which indicates the production of superoxide radical [$O2^{\bullet-}$] [133], according to the following equation in Scheme 16:

$$\boldsymbol{p-BQ} \xleftrightarrow{O2-,\,H+} \boldsymbol{QH} \xleftrightarrow{O2-,\,H+} \boldsymbol{H2Q} \qquad \textit{Scheme 116}$$

If the $O_2^{\bullet-}$ radical is involved in the oxidation of TMB, the presence of p-BQ would reduce the level of $O_2^{\bullet-}$ radicals, thus decreasing the reaction rate. However, the results showed that there was no significant difference in reaction rate between samples with and without p-BQ with p-values of 0.483, 0.275, and0.256 for tested concentrations of 40, 80, and 160 µg/ml, respectively, suggesting that there is no superoxide radical production.

It has been documented that the peroxidase reaction mechanism may involve the electron transfer process. The determination of the electron transfer process can be accomplished by examining the conversion of reduced Cytochrome C to oxidized Cytochrome C. Reduced Cytochrome C displays two peaks at 520 nm and 550 nm, while the oxidized form of Cytochrome C, after losing electrons, exhibits the disappearance of these two peaks and a newly developed peak at 530 nm.

The results confirm the involvement of the electron transfer process in the peroxidase-like activity of HEN. The suggested pathway involves HEN initially attaching to the surface, with the lone-pair electrons from TMB donating to HEN, leading to an increase in the electron density of HEN. Subsequently, HEN, which is electron-rich, transfers electrons to nearby molecules of H_2O_2, thus accelerating the electron transfer process that occurs between TMB and HEN. Finally, as part of this catalytic cycle, TMB undergoes oxidation to produce a blue derivative, while H_2O_2 is reduced to water under acidic conditions [55]. The pathway could be described as follows in Scheme 17, where H_2O_2 is considered an electron acceptor:

$$\mathbf{H_2O_2 + 2H^+ + 2e^- \rightarrow 2H_2O} \qquad \textit{Scheme 17}$$

Several studies showed multi-metallic nanozymes may play multienzyme-like activity [134], therefore, in this thesis, the Catalase-like activity of HEN was also investigated.

In this study, an approach based on the Europium-tetracycline complex (EuTc) was used to detect the catalase activity of HEN. The EuTc is a weak fluorescent complex with a maximum emission at 615 nm. However, upon the addition of hydrogen peroxide, a new complex (EuTc-

HP) is formed, which exhibits 15-fold higher fluorescence intensity [135]. The concept behind this experiment is if HEN displays catalase-like activity, it will decompose EuTc-HP into EuTc, then reduce the fluorescent signal.

As expected, HEN shows a significant reduction in fluorescence intensity, which increased proportionally with the increase of HEN concentrations. The reduction in fluorescence intensity measured was 14.56%, 22.99%, 34.97%, and 45.43% for 20, 40, 80, and 160 µg/ml of HEN respectively, while negative control showed only a 7.85% reduction of fluorescence intensity, and native catalase enzyme exhibited 34.38% reduction, which is almost equivalent to the catalase-like activity of 80 µg/ml HEN.

V. Conclusion

Nanozymes have been recognized as a promising alternative to natural enzymes due to their distinct properties, including high catalytic activity, robustness under harsh conditions, cost-effectiveness, and multifunctionality, among other advantages. Thus, exploring and optimizing nanozymes has become a crucial area of research in the fields of nanotechnology and biomedicine. High-entropy oxides have emerged as a particularly promising candidate for multienzyme catalysis due to their unique composition and characteristics.

In this thesis, a specific high-entropy oxide, $(FeCr)(CuFeMn)_2O_4$, was evaluated for its potential as a multienzyme catalyst. The results of the experiment demonstrated its peroxidase-like activity, which was 3.6 times faster catalytic reaction rate than that of Fe_3O_4-NP, and showed 2.6 times higher substrate affinity than that of HRP. It was also determined that the electron transfer process was involved in the oxidation of TMB, rather than the formation of free radicals. Additionally, the materials also displayed catalase-like activity in a concentration manner in which a concentration of 80 µg/ml of HEN produced a comparable performance to native catalase.

Further investigation of the multienzyme-like activity of $(FeCr)(CuFeMn)_2O_4$ (HEN) could provide valuable insights into its potential applications as a nanozyme. For instance, it is important to determine whether HEN possesses superoxide dismutase or oxidase-like activities, as these properties could be used in further applications.

Another crucial area of research is to assess whether HEN can be reused efficiently without losing its catalytic activity, which would enhance its cost-effectiveness and practical utility. Additionally, determining the lowest limit of detection for H_2O_2 by HEN is essential for its potential applications in biomedical and environmental monitoring.

Thus, future studies on HEN enzyme-like activities could focus on answering these questions, which would provide a more comprehensive understanding of its properties and potential applications.

Foot Notes:

*Reactive Oxygen Species (ROS): this term describes the molecules that are produced by peroxidase or oxidase enzymes and possess a highly oxidizing activity. Hydroxyl radical and superoxide anion radical is considered the most well-known representatives of ROS, they can harm the cell after accumulation to a high extent leading to cell death or harmful incidences, therefore ROS are linked somehow with aging and neurodegenerative diseases [136].

**Fenton reaction: is a chemical process that involves the reaction of hydrogen peroxide with a ferrous ion (Fe^{2+}) at low pH media. The reaction results in the formation of hydroxyl radicals (•OH) and ferric ions (Fe^{3+}), which are highly reactive and can initiate various oxidation processes.

VI. References

[1] M. Garcia-Viloca, J. Gao, M. Karplus, D.G. Truhlar, How enzymes work: analysis by modern rate theory and computer simulations, Science. 303 (2004) 186–195. https://doi.org/10.1126/SCIENCE.1088172.

[2] Y. Lin, J. Ren, X. Qu, Catalytically active nanomaterials: A promising candidate for artificial enzymes, Acc Chem Res. 47 (2014) 1097–1105. https://doi.org/10.1021/AR400250Z/ASSET/IMAGES/MEDIUM/AR-2013-00250Z_0012.GIF.

[3] K. Korschelt, M.N. Tahir, W. Tremel, A Step into the Future: Applications of Nanoparticle Enzyme Mimics, Chemistry – A European Journal. 24 (2018) 9703–9713. https://doi.org/10.1002/CHEM.201800384.

[4] J. Wu, X. Wang, Q. Wang, Z. Lou, S. Li, Y. Zhu, L. Qin, H. Wei, Nanomaterials with enzyme-like characteristics (nanozymes): next-generation artificial enzymes (II), Chem Soc Rev. 48 (2019) 1004–1076. https://doi.org/10.1039/C8CS00457A.

[5] N.A. Kotov, Chemistry. Inorganic nanoparticles as protein mimics, Science. 330 (2010) 188–189. https://doi.org/10.1126/SCIENCE.1190094.

[6] M. Liang, X. Yan, Nanozymes: From New Concepts, Mechanisms, and Standards to Applications, Acc Chem Res. 52 (2019) 2190–2200. https://doi.org/10.1021/acs.accounts.9b00140.

[7] F. Manea, F.B. Houillon, L. Pasquato, P. Scrimin, Nanozymes: gold-nanoparticle-based transphosphorylation catalysts, Angew Chem Int Ed Engl. 43 (2004) 6165–6169. https://doi.org/10.1002/ANIE.200460649.

[8] L. Gao, J. Zhuang, L. Nie, J. Zhang, Y. Zhang, N. Gu, T. Wang, J. Feng, D. Yang, S. Perrett, X. Yan, Intrinsic peroxidase-like activity of ferromagnetic nanoparticles, Nat Nanotechnol. 2 (2007) 577–583. https://doi.org/10.1038/nnano.2007.260.

[9] Y. Ai, Z. Hu, L. Liu, J. Zhou, Y. Long, J. Li, M. Ding, H. Bin Sun, Q. Liang, Magnetically Hollow Pt Nanocages with Ultrathin Walls as a Highly Integrated Nanoreactor for Catalytic Transfer Hydrogenation Reaction, Advanced Science. 6 (2019). https://doi.org/10.1002/ADVS.201802132.

[10] J. Wu, J. Zhang, Y. Ai, J. Li, X. Zhang, Z.N. Hu, H. Wang, Q. Liang, H. Bin Sun, Cobalt-promoted fabrication of 3D carbon with a nanotube-sheet mutual support structure: scalable preparation of a high-performance anode material for Li-ion batteries, Nanotechnology. 31 (2019) 085402. https://doi.org/10.1088/1361-6528/AB5477.

[11] S. Ren, Y. Ai, X. Zhang, M. Ruan, Z.N. Hu, L. Liu, J. Li, Y. Wang, J.X. Liang, H. Jia, Y.Y. Liu, D. Niu, H. Bin Sun, Q. Liang, Recycling Antimony(III) by Magnetic Carbon Nanospheres: Turning Waste to Recoverable Catalytic for Synthesis of Esters and Triazoles, ACS Sustain Chem Eng. 8 (2020) 469–477. https://doi.org/10.1021/ACSSUSCHEMENG.9B05802/SUPPL_FILE/SC9B05802_SI_001.PDF.

[12] A.A. Vernekar, T. Das, S. Ghosh, G. Mugesh, A Remarkably Efficient MnFe2O4-based Oxidase Nanozyme, Chem Asian J. 11 (2016) 72–76. https://doi.org/10.1002/asia.201500942.

[13] L. Liu, Y. Liu, Y. Ai, J. Li, J. Zhou, Z. Fan, H. Bao, R. Jiang, Z. Hu, J. Wang, K. Jing, Y. Wang, Q. Liang, H. Sun, Pd-CuFe Catalyst for Transfer Hydrogenation of Nitriles: Controllable Selectivity

to Primary Amines and Secondary Amines, IScience. 8 (2018) 61–73. https://doi.org/10.1016/J.ISCI.2018.09.010.

[14] X. Mu, J. Wang, H. He, Q. Li, B. Yang, J. Wang, H. Liu, Y. Gao, L. Ouyang, S. Sun, Q. Ren, X. Shi, W. Hao, Q. Fei, J. Yang, L. Li, R. Vest, T. Wyss-Coray, J. Luo, X.D. Zhang, An oligomeric semiconducting nanozyme with ultrafast electron transfers alleviates acute brain injury, Sci Adv. 7 (2021) 1210. https://doi.org/10.1126/SCIADV.ABK1210.

[15] Y. Ai, M. He, F. Zhang, Y. Long, Y. Li, Q. Han, M. Ding, H. Bin Sun, Q. Liang, Metallo-supramolecular polymer engineered porous carbon framework encapsulated stable ultra-small nanoparticles: a general approach to construct highly dispersed catalysts, J Mater Chem A Mater. 6 (2018) 16680–16689. https://doi.org/10.1039/C8TA05369C.

[16] Z. Song, C. Jiang, F. Wang, L. Yu, S. Ye, P. Dramou, H. He, Nanozyme based on graphene oxide modified with Fe3O4, CuO, and cucurbit[6]uril for colorimetric determination of homocysteine, Microchimica Acta. 188 (2021) 1–10. https://doi.org/10.1007/S00604-021-04868-0/TABLES/2.

[17] L. Yao, M.M. Zhao, Q.W. Luo, Y.C. Zhang, T.T. Liu, Z. Yang, M. Liao, P. Tu, K.W. Zeng, Carbon Quantum Dots-Based Nanozyme from Coffee Induces Cancer Cell Ferroptosis to Activate Antitumor Immunity, ACS Nano. 16 (2022) 9228–9239. https://doi.org/10.1021/ACSNANO.2C01619/SUPPL_FILE/NN2C01619_SI_001.PDF.

[18] P. Rozhin, J. Abdel Monem Gamal, S. Giordani, S. Marchesan, Carbon Nanomaterials (CNMs) and Enzymes: From Nanozymes to CNM-Enzyme Conjugates and Biodegradation, Materials. 15 (2022). https://doi.org/10.3390/MA15031037.

[19] Y. Liu, K. Ai, X. Ji, D. Askhatova, R. Du, L. Lu, J. Shi, Comprehensive Insights into the Multi-Antioxidative Mechanisms of Melanin Nanoparticles and Their Application To Protect Brain from Injury in Ischemic Stroke, J Am Chem Soc. 139 (2017) 856–862. https://doi.org/10.1021/JACS.6B11013.

[20] W. Kong, X. Guo, M. Jing, F. Qu, L. Lu, Highly sensitive photoelectrochemical detection of bleomycin based on Au/WS2 nanorod array as signal matrix and Ag/ZnMOF nanozyme as multifunctional amplifier, Biosens Bioelectron. 150 (2020) 111875. https://doi.org/10.1016/J.BIOS.2019.111875.

[21] Y. Huang, M. Zhao, S. Han, Z. Lai, J. Yang, C. Tan, Q. Ma, Q. Lu, J. Chen, X. Zhang, Z. Zhang, B. Li, B. Chen, Y. Zong, H. Zhang, Growth of Au Nanoparticles on 2D Metalloporphyrinic Metal-Organic Framework Nanosheets Used as Biomimetic Catalysts for Cascade Reactions, Adv Mater. 29 (2017). https://doi.org/10.1002/ADMA.201700102.

[22] M. Lian, Z. Xue, X. Qiao, C. Liu, S. Zhang, X. Li, C. Huang, Q. Song, W. Yang, X. Chen, T. Wang, Movable Hollow Nanoparticles as Reactive Oxygen Scavengers, Chem. 5 (2019) 2378–2387. https://doi.org/10.1016/J.CHEMPR.2019.05.023.

[23] Q. Wu, Z. He, X. Wang, Q. Zhang, Q. Wei, S. Ma, C. Ma, J. Li, Q. Wang, Cascade enzymes within self-assembled hybrid nanogel mimicked neutrophil lysosomes for singlet oxygen elevated cancer therapy, Nature Communications 2019 10:1. 10 (2019) 1–14. https://doi.org/10.1038/s41467-018-08234-2.

[24] Y. Jiang, X. Zhao, J. Huang, J. Li, P.K. Upputuri, H. Sun, X. Han, M. Pramanik, Y. Miao, H. Duan, K. Pu, R. Zhang, Transformable hybrid semiconducting polymer nanozyme for second near-

infrared photothermal ferrotherapy, Nature Communications 2020 11:1. 11 (2020) 1–13. https://doi.org/10.1038/s41467-020-15730-x.

[25] R. Singh, A.S. Karakoti, W. Self, S. Seal, S. Singh, Redox-sensitive cerium oxide nanoparticles protect human keratinocytes from oxidative stress induced by glutathione depletion, Langmuir. 32 (2016) 12202–12211. https://doi.org/10.1021/ACS.LANGMUIR.6B03022/SUPPL_FILE/LA6B03022_SI_001.PDF.

[26] P. Patel, K. Kansara, R. Singh, R.K. Shukla, S. Singh, A. Dhawan, A. Kumar, Cellular internalization and antioxidant activity of cerium oxide nanoparticles in human monocytic leukemia cells, Int J Nanomedicine. 13 (2018) 39–41. https://doi.org/10.2147/IJN.S124996.

[27] A. Dhall, W. Self, Cerium Oxide Nanoparticles: A Brief Review of Their Synthesis Methods and Biomedical Applications, Antioxidants (Basel). 7 (2018). https://doi.org/10.3390/ANTIOX7080097.

[28] V. Leifeld, T.P.M. dos Santos, D.W. Zelinski, L. Igarashi-Mafra, Ferrous ions reused as catalysts in Fenton-like reactions for remediation of agro-food industrial wastewater, J Environ Manage. 222 (2018) 284–292. https://doi.org/10.1016/J.JENVMAN.2018.05.087.

[29] J. Mu, Y. Wang, M. Zhao, L. Zhang, Intrinsic peroxidase-like activity and catalase-like activity of Co3O4 nanoparticles, Chemical Communications. 48 (2012) 2540–2542. https://doi.org/10.1039/c2cc17013b.

[30] J. Mu, Y. Wang, M. Zhao, L. Zhang, Intrinsic peroxidase-like activity and catalase-like activity of Co 3 O 4 nanoparticles, 2012.

[31] J. Fan, J.J. Yin, B. Ning, X. Wu, Y. Hu, M. Ferrari, G.J. Anderson, J. Wei, Y. Zhao, G. Nie, Direct evidence for catalase and peroxidase activities of ferritin-platinum nanoparticles, Biomaterials. 32 (2011) 1611–1618. https://doi.org/10.1016/j.biomaterials.2010.11.004.

[32] S. Bhagat, N. v. Srikanth Vallabani, V. Shutthanandan, M. Bowden, A.S. Karakoti, S. Singh, Gold core/ceria shell-based redox active nanozyme mimicking the biological multienzyme complex phenomenon, J Colloid Interface Sci. 513 (2018) 831–842. https://doi.org/10.1016/J.JCIS.2017.11.064.

[33] R. Singh, S. Singh, Redox-dependent catalase mimetic cerium oxide-based nanozyme protect human hepatic cells from 3-AT induced acatalasemia, Colloids Surf B Biointerfaces. 175 (2019) 625–635. https://doi.org/10.1016/J.COLSURFB.2018.12.042.

[34] Z. Chen, J.J. Yin, Y.T. Zhou, Y. Zhang, L. Song, M. Song, S. Hu, N. Gu, Dual enzyme-like activities of iron oxide nanoparticles and their implication for diminishing cytotoxicity, ACS Nano. 6 (2012) 4001–4012. https://doi.org/10.1021/NN300291R.

[35] A. Rahal, A. Kumar, V. Singh, B. Yadav, R. Tiwari, S. Chakraborty, K. Dhama, Oxidative stress, prooxidants, and antioxidants: the interplay, Biomed Res Int. 2014 (2014). https://doi.org/10.1155/2014/761264.

[36] V. Urbanova, M. Magro, A. Gedanken, D. Baratella, F. Vianello, R. Zboril, Nanocrystalline iron oxides, composites, and related materials as a platform for electrochemical, magnetic, and chemical biosensors, Chemistry of Materials. 26 (2014) 6653–6673. https://doi.org/10.1021/CM500364X/ASSET/IMAGES/MEDIUM/CM-2014-00364X_0037.GIF.

[37] K. Shah, S. Bhagat, D. Varade, S. Singh, Novel synthesis of polyoxyethylene cholesteryl ether coated Fe-Pt nanoalloys: A multifunctional and cytocompatible bimetallic alloy exhibiting intrinsic chemical catalysis and biological enzyme-like activities, Colloids Surf A Physicochem Eng Asp. 553 (2018) 50–57. https://doi.org/10.1016/J.COLSURFA.2018.05.034.

[38] W. Luo, C. Zhu, S. Su, D. Li, Y. He, Q. Huang, C. Fan, Self-catalyzed, self-limiting growth of glucose oxidase-mimicking gold nanoparticles, ACS Nano. 4 (2010) 7451–7458. https://doi.org/10.1021/NN102592H/SUPPL_FILE/NN102592H_SI_001.PDF.

[39] A. Asati, C. Kaittanis, S. Santra, J.M. Perez, pH-tunable oxidase-like activity of cerium oxide nanoparticles achieving sensitive fluorigenic detection of cancer biomarkers at neutral pH, Anal Chem. 83 (2011) 2547–2553. https://doi.org/10.1021/AC102826K.

[40] Y. Wan, P. Qi, D. Zhang, J. Wu, Y. Wang, Manganese oxide nanowire-mediated enzyme-linked immunosorbent assay, Biosens Bioelectron. 33 (2012) 69–74. https://doi.org/10.1016/J.BIOS.2011.12.033.

[41] A. Strzepa, K.A. Pritchard, B.N. Dittel, Myeloperoxidase: A new player in autoimmunity, Cell Immunol. 317 (2017) 1–8. https://doi.org/10.1016/J.CELLIMM.2017.05.002.

[42] H. Wei, E. Wang, Fe3O4 magnetic nanoparticles as peroxidase mimetics and their applications in H2O2 and glucose detection, Anal Chem. 80 (2008) 2250–2254. https://doi.org/10.1021/ac702203f.

[43] J.W. Zhang, H.T. Zhang, Z.Y. Du, X. Wang, S.H. Yu, H.L. Jiang, Water-stable metal–organic frameworks with intrinsic peroxidase-like catalytic activity as a colorimetric biosensing platform, Chemical Communications. 50 (2014) 1092–1094. https://doi.org/10.1039/c3cc48398c.

[44] Z. Dai, S. Liu, J. Bao, H. Ju, Nanostructured FeS as a mimic peroxidase for biocatalysis and biosensing, Chemistry. 15 (2009) 4321–4326. https://doi.org/10.1002/CHEM.200802158.

[45] J. Shah, R. Purohit, R. Singh, A.S. Karakoti, S. Singh, ATP-enhanced peroxidase-like activity of gold nanoparticles, J Colloid Interface Sci. 456 (2015) 100–107. https://doi.org/10.1016/j.jcis.2015.06.015.

[46] G. Nie, L. Zhang, J. Lei, L. Yang, Z. Zhang, X. Lu, C. Wang, Monocrystalline VO2 (B) nanobelts: large-scale synthesis, intrinsic peroxidase-like activity and application in biosensing, J Mater Chem A Mater. 2 (2014) 2910–2914. https://doi.org/10.1039/C3TA15051H.

[47] K. Sobańska, P. Pietrzyk, Z. Sojka, Generation of Reactive Oxygen Species via Electroprotic Interaction of H2O2 with ZrO2 Gel: Ionic Sponge Effect and pH-Switchable Peroxidase- and Catalase-Like Activity, ACS Catal. 7 (2017) 2935–2947. https://doi.org/10.1021/ACSCATAL.7B00189.

[48] A.K. Dutta, S.K. Maji, D.N. Srivastava, A. Mondal, P. Biswas, P. Paul, B. Adhikary, Synthesis of FeS and FeSe nanoparticles from a single source precursor: a study of their photocatalytic activity, peroxidase-like behavior, and electrochemical sensing of H2O2, ACS Appl Mater Interfaces. 4 (2012) 1919–1927. https://doi.org/10.1021/AM300408R.

[49] H. Su, D.D. Liu, M. Zhao, W.L. Hu, S.S. Xue, Q. Cao, X.Y. Le, L.N. Ji, Z.W. Mao, Dual-enzyme characteristics of polyvinylpyrrolidone-capped iridium nanoparticles and their cellular

protective effect against H2O2-induced oxidative damage, ACS Appl Mater Interfaces. 7 (2015) 8233–8242. https://doi.org/10.1021/acsami.5b01271.

[50] T.M. Chen, X.J. Wu, J.X. Wang, G.W. Yang, WSe2 few layers with enzyme mimic activity for high-sensitive and high-selective visual detection of glucose, Nanoscale. 9 (2017) 11806–11813. https://doi.org/10.1039/c7nr03179c.

[51] Y. Jv, B. Li, R. Cao, Positively-charged gold nanoparticles as peroxidiase mimic and their application in hydrogen peroxide and glucose detection, Chemical Communications. 46 (2010) 8017–8019. https://doi.org/10.1039/c0cc02698k.

[52] X. Zuo, C. Peng, Q. Huang, S. Song, L. Wang, D. Li, C. Fan, Design of a carbon nanotube/magnetic nanoparticle-based peroxidase-like nanocomplex and its application for highly efficient catalytic oxidation of phenols, Nano Res. 2 (2009) 617–623. https://doi.org/10.1007/s12274-009-9062-3.

[53] K. Herget, P. Hubach, S. Pusch, P. Deglmann, H. Götz, T.E. Gorelik, I.A. Gural'skiy, F. Pfitzner, T. Link, S. Schenk, M. Panthöfer, V. Ksenofontov, U. Kolb, T. Opatz, R. André, W. Tremel, Haloperoxidase Mimicry by CeO2-x Nanorods Combats Biofouling, Adv Mater. 29 (2017). https://doi.org/10.1002/ADMA.201603823.

[54] J. Li, G. Zhang, L. Wang, A. Shen, J. Hu, Simultaneous enzymatic and SERS properties of bifunctional chitosan-modified popcorn-like Au-Ag nanoparticles for high sensitive detection of melamine in milk powder, (n.d.). https://doi.org/10.1016/j.talanta.2015.03.050.

[55] T.M. Chen, X.J. Wu, J.X. Wang, G.W. Yang, WSe2 few layers with enzyme mimic activity for high-sensitive and high-selective visual detection of glucose, Nanoscale. 9 (2017) 11806–11813. https://doi.org/10.1039/c7nr03179c.

[56] V.R. Mate, M. Shirai, C. V. Rode, Heterogeneous Co3O4 catalyst for selective oxidation of aqueous veratryl alcohol using molecular oxygen, Catal Commun. 33 (2013) 66–69. https://doi.org/10.1016/j.catcom.2012.12.015.

[57] D. Xu, L. Wu, H. Yao, L. Zhao, D. Xu, L. Wu, H. Yao, L. Zhao, 2203400 (1 of 22) Catalase-Like Nanozymes: Classification, Catalytic Mechanisms, and Their Applications, (2022). https://doi.org/10.1002/smll.202203400.

[58] I. Celardo, J.Z. Pedersen, E. Traversa, L. Ghibelli, Pharmacological potential of cerium oxide nanoparticles, Nanoscale. 3 (2011) 1411–1420. https://doi.org/10.1039/c0nr00875c.

[59] M. Gao, X. Lu, M. Chi, S. Chen, C. Wang, Fabrication of oxidase-like hollow MnCo2O4 nanofibers and their sensitive colorimetric detection of sulfite and L-cysteine, Inorg Chem Front. 4 (2017) 1862–1869. https://doi.org/10.1039/C7QI00458C.

[60] H. Wang, K. Wan, X. Shi, Recent Advances in Nanozyme Research, Advanced Materials. 31 (2019). https://doi.org/10.1002/ADMA.201805368.

[61] G. Vinothkumar, P. Arunkumar, A. Mahesh, A. Dhayalan, K. Suresh Babu, Size- and defect-controlled anti-oxidant enzyme mimetic and radical scavenging properties of cerium oxide nanoparticles, New Journal of Chemistry. 42 (2018) 18810–18823. https://doi.org/10.1039/C8NJ04435J.

[62] R. Long, K. Mao, X. Ye, W. Yan, Y. Huang, J. Wang, Y. Fu, X. Wang, X. Wu, Y. Xie, Y. Xiong, Surface facet of palladium nanocrystals: A key parameter to the activation of molecular

oxygen for organic catalysis and cancer treatment, J Am Chem Soc. 135 (2013) 3200–3207. https://doi.org/10.1021/JA311739V/SUPPL_FILE/JA311739V_SI_001.PDF.

[63] X. Zhang, Y. Huang, Evaluation of the antioxidant activity of phenols and tannic acid determination with Mn3O4 nano-octahedrons as an oxidase mimic, Analytical Methods. 7 (2015) 8640–8646. https://doi.org/10.1039/C5AY01732G.

[64] S.S. Ali, J.I. Hardt, K.L. Quick, J. Sook Kim-Han, B.F. Erlanger, T.T. Huang, C.J. Epstein, L.L. Dugan, A biologically effective fullerene (C60) derivative with superoxide dismutase mimetic properties, Free Radic Biol Med. 37 (2004) 1191–1202. https://doi.org/10.1016/J.FREERADBIOMED.2004.07.002.

[65] C. Korsvik, S. Patil, S. Seal, W.T. Self, Superoxide dismutase mimetic properties exhibited by vacancy engineered ceria nanoparticles, Chemical Communications. (2007) 1056–1058. https://doi.org/10.1039/B615134E.

[66] Y. Liu, G. Zhu, J. Yang, A. Yuan, X. Shen, Peroxidase-Like Catalytic Activity of Ag3PO4 Nanocrystals Prepared by a Colloidal Route, PLoS One. 9 (2014) e109158. https://doi.org/10.1371/JOURNAL.PONE.0109158.

[67] C. Lu, X. Liu, Y. Li, F. Yu, L. Tang, Y. Hu, Y. Ying, Multifunctional Janus Hematite-Silica Nanoparticles: Mimicking Peroxidase-Like Activity and Sensitive Colorimetric Detection of Glucose, ACS Appl Mater Interfaces. 7 (2015) 15395–15402. https://doi.org/10.1021/ACSAMI.5B03423/SUPPL_FILE/AM5B03423_SI_001.PDF.

[68] H. Zhang, N. Toshima, Glucose oxidation using Au-containing bimetallic and trimetallic nanoparticles, Catal Sci Technol. 3 (2013) 268–278. https://doi.org/10.1039/C2CY20345F.

[69] X. Chen, X. Tian, B. Su, Z. Huang, X. Chen, M. Oyama, Au nanoparticles on citrate-functionalized graphene nanosheets with a high peroxidase-like performance, Dalton Transactions. 43 (2014) 7449–7454. https://doi.org/10.1039/C3DT53316F.

[70] S. Indrawirawan, H. Sun, X. Duan, S. Wang, Low temperature combustion synthesis of nitrogen-doped graphene for metal-free catalytic oxidation, J Mater Chem A Mater. 3 (2015) 3432–3440. https://doi.org/10.1039/C4TA05940A.

[71] N.V.S. Vallabani, A.S. Karakoti, S. Singh, ATP-mediated intrinsic peroxidase-like activity of Fe3O4-based nanozyme: One step detection of blood glucose at physiological pH, Colloids Surf B Biointerfaces. 153 (2017) 52–60. https://doi.org/10.1016/J.COLSURFB.2017.02.004.

[72] J. Li, W. Liu, X. Wu, X. Gao, Mechanism of pH-switchable peroxidase and catalase-like activities of gold, silver, platinum and palladium, Biomaterials. 48 (2015) 37–44. https://doi.org/10.1016/J.BIOMATERIALS.2015.01.012.

[73] N. Singh, M.A. Savanur, S. Srivastava, P. D'Silva, G. Mugesh, A Redox Modulatory Mn3O4 Nanozyme with Multi-Enzyme Activity Provides Efficient Cytoprotection to Human Cells in a Parkinson's Disease Model, Angewandte Chemie. 129 (2017) 14455–14459. https://doi.org/10.1002/ANGE.201708573.

[74] C. Wang, Y. Shi, Y.Y. Dan, X.G. Nie, J. Li, X.H. Xia, Enhanced Peroxidase-Like Performance of Gold Nanoparticles by Hot Electrons, Chemistry - A European Journal. 23 (2017) 6717–6723. https://doi.org/10.1002/chem.201605380.

[75] Z. Zhang, Y. Li, X. Zhang, J. Liu, Molecularly imprinted nanozymes with faster catalytic activity and better specificity, Nanoscale. 11 (2019) 4854–4863. https://doi.org/10.1039/C8NR09816F.

[76] Y. Hu, S. Feng, F. Gao, E.C.Y. Li-Chan, E. Grant, X. Lu, Detection of melamine in milk using molecularly imprinted polymers–surface enhanced Raman spectroscopy, Food Chem. 176 (2015) 123–129. https://doi.org/10.1016/J.FOODCHEM.2014.12.051.

[77] L. Guo, H. Zheng, C. Zhang, L. Qu, L. Yu, A novel molecularly imprinted sensor based on PtCu bimetallic nanoparticle deposited on PSS functionalized graphene with peroxidase-like activity for selective determination of puerarin, Talanta. 210 (2020) 120621. https://doi.org/10.1016/J.TALANTA.2019.120621.

[78] X. Xia, J. Zhang, N. Lu, M.J. Kim, K. Ghale, Y. Xu, E. McKenzie, J. Liu, H. Ye, Pd-Ir Core-Shell Nanocubes: A Type of Highly Efficient and Versatile Peroxidase Mimic, ACS Nano. 9 (2015) 9994–10004. https://doi.org/10.1021/acsnano.5b03525.

[79] J. Wang, P. Wang, Q. Zhao, J. Shi, T. Yu, X. Du, X. Hao, A. Abudula, G. Guan, Stable hetero-metal doped Co-based catalysts prepared by electrodeposition method for low temperature combustion of toluene, Carbon Resources Conversion. 3 (2020) 95–103. https://doi.org/10.1016/J.CRCON.2020.04.001.

[80] Y. Wang, H. Li, L. Guo, Q. Jiang, F. Liu, A cobalt-doped iron oxide nanozyme as a highly active peroxidase for renal tumor catalytic therapy, RSC Adv. 9 (2019) 18815–18822. https://doi.org/10.1039/C8RA05487H.

[81] X. Sun, S. Guo, C.S. Chung, W. Zhu, S. Sun, A Sensitive H2O2 Assay Based on Dumbbell-like PtPd-Fe3O4 Nanoparticles, Advanced Materials. 25 (2013) 132–136. https://doi.org/10.1002/ADMA.201203218.

[82] C. Qi, S. Cai, X. Wang, J. Li, Z. Lian, S. Sun, R. Yang, C. Wang, Enhanced oxidase/peroxidase-like activities of aptamer conjugated MoS 2 /PtCu nanocomposites and their biosensing application †, (2016). https://doi.org/10.1039/c6ra03507h.

[83] K. Qu, P. Shi, J. Ren, X. Qu, Nanocomposite Incorporating V2O5 Nanowires and Gold Nanoparticles for Mimicking an Enzyme Cascade Reaction and Its Application in the Detection of Biomolecules, Chemistry – A European Journal. 20 (2014) 7501–7506. https://doi.org/10.1002/CHEM.201400309.

[84] X. Meng, K. Fan, X. Yan, Nanozymes: an emerging field bridging nanotechnology and enzymology, Sci China Life Sci. 62 (2019) 1543–1546. https://doi.org/10.1007/S11427-019-1557-8/METRICS.

[85] L. Panzella, G. Gentile, G. D'Errico, N.F. Della Vecchia, M.E. Errico, A. Napolitano, C. Carfagna, M. D'Ischia, Atypical structural and π-electron features of a melanin polymer that lead to superior free-radical-scavenging properties, Angew Chem Int Ed Engl. 52 (2013) 12684–12687. https://doi.org/10.1002/ANIE.201305747.

[86] Y. Ding, B. Yang, H. Liu, Z. Liu, X. Zhang, X. Zheng, Q. Liu, FePt-Au ternary metallic nanoparticles with the enhanced peroxidase-like activity for ultrafast colorimetric detection of H 2 O 2, Sensors and Actuators B. 259 (2018) 775–783. https://doi.org/10.1016/j.snb.2017.12.115.

[87] K. Zhang, W. Zuo, Z. Wang, J. Liu, T. Li, B. Wang, Z. Yang, A simple route to CoFe 2 O 4 nanoparticles with shape and size control and their tunable peroxidase-like activity †, (2015). https://doi.org/10.1039/c4ra15675g.

[88] Facile method to synthesize dopamine-capped mixed ferrite nanoparticles and their peroxidase-like activity, (2017). https://doi.org/10.1088/1361-6463/aa5bf6.

[89] B. Wang, P. Ju, D. Zhang, X. Han, L. Zheng, X. Yin, C. Sun, Colorimetric detection of H2O2 using flower-like Fe2(MoO4)3 microparticles as a peroxidase mimic, Microchimica Acta. 183 (2016) 3025–3033. https://doi.org/10.1007/S00604-016-1955-8/FIGURES/4.

[90] C. Wang, J. Qian, K. Wang, X. Yang, Q. Liu, N. Hao, C. Wang, X. Dong, X. Huang, Colorimetric aptasensing of ochratoxin A using Au@Fe 3 O 4 nanoparticles as signal indicator and magnetic separator, (n.d.). https://doi.org/10.1016/j.bios.2015.11.004.

[91] S. Das, C.J. Neal, J. Ortiz, S. Seal, Engineered nanoceria cytoprotection in vivo: mitigation of reactive oxygen species and double-stranded DNA breakage due to radiation exposure, Nanoscale. 10 (2018) 21069–21075. https://doi.org/10.1039/C8NR04640A.

[92] M. Soh, D.W. Kang, H.G. Jeong, D. Kim, D.Y. Kim, W. Yang, C. Song, S. Baik, I.Y. Choi, S.K. Ki, H.J. Kwon, T. Kim, C.K. Kim, S.H. Lee, T. Hyeon, Ceria–Zirconia Nanoparticles as an Enhanced Multi-Antioxidant for Sepsis Treatment, Angewandte Chemie - International Edition. 56 (2017) 11399–11403. https://doi.org/10.1002/ANIE.201704904.

[93] W. Li, Z. Liu, C. Liu, Y. Guan, J. Ren, X. Qu, Manganese Dioxide Nanozymes as Responsive Cytoprotective Shells for Individual Living Cell Encapsulation, Angew Chem Int Ed Engl. 56 (2017) 13661–13665. https://doi.org/10.1002/ANIE.201706910.

[94] H. Wu, L. Liu, L. Song, M. Ma, N. Gu, Y. Zhang, Enhanced Tumor Synergistic Therapy by Injectable Magnetic Hydrogel Mediated Generation of Hyperthermia and Highly Toxic Reactive Oxygen Species, ACS Nano. 13 (2019) 14013–14023. https://doi.org/10.1021/ACSNANO.9B06134/SUPPL_FILE/NN9B06134_SI_001.PDF.

[95] Y. Yao, D. Wang, J. Hu, X. Yang, Tumor-targeting inorganic nanomaterials synthesized by living cells, Nanoscale Adv. 3 (2021) 2975–2994. https://doi.org/10.1039/D1NA00155H.

[96] Z. Chen, H. Ji, C. Liu, W. Bing, Z. Wang, X. Qu, A Multinuclear Metal Complex Based DNase-Mimetic Artificial Enzyme: Matrix Cleavage for Combating Bacterial Biofilms, Angewandte Chemie International Edition. 55 (2016) 10732–10736. https://doi.org/10.1002/ANIE.201605296.

[97] J. Shan, X. Li, K. Yang, W. Xiu, Q. Wen, Y. Zhang, L. Yuwen, L. Weng, Z. Teng, L. Wang, Efficient Bacteria Killing by Cu2WS4 Nanocrystals with Enzyme-like Properties and Bacteria-Binding Ability, ACS Nano. 13 (2019) 13797–13808. https://doi.org/10.1021/ACSNANO.9B03868.

[98] Z. Wang, K. Dong, Z. Liu, Y. Zhang, Z. Chen, H. Sun, J. Ren, X. Qu, Activation of biologically relevant levels of reactive oxygen species by Au/g-C3N4 hybrid nanozyme for bacteria killing and wound disinfection, Biomaterials. 113 (2017) 145–157. https://doi.org/10.1016/J.BIOMATERIALS.2016.10.041.

[99] Y. Zhang, P. Sun, L. Zhang, Z. Wang, F. Wang, K. Dong, Z. Liu, J. Ren, X. Qu, Silver-Infused Porphyrinic Metal–Organic Framework: Surface-Adaptive, On-Demand Nanoplatform for

Synergistic Bacteria Killing and Wound Disinfection, Adv Funct Mater. 29 (2019) 1808594. https://doi.org/10.1002/ADFM.201808594.

[100] C.N. Loynachan, A.P. Soleimany, J.S. Dudani, Y. Lin, A. Najer, A. Bekdemir, Q. Chen, S.N. Bhatia, M.M. Stevens, Renal clearable catalytic gold nanoclusters for in vivo disease monitoring, Nat Nanotechnol. 14 (2019) 883–890. https://doi.org/10.1038/S41565-019-0527-6.

[101] D. Li, B. Liu, P.J.J. Huang, Z. Zhang, J. Liu, Highly active fluorogenic oxidase-mimicking NiO nanozymes, Chemical Communications. 54 (2018) 12519–12522. https://doi.org/10.1039/C8CC07062H.

[102] J.W. Yeh, S.K. Chen, S.J. Lin, J.Y. Gan, T.S. Chin, T.T. Shun, C.H. Tsau, S.Y. Chang, Nanostructured high-entropy alloys with multiple principal elements: Novel alloy design concepts and outcomes, Adv Eng Mater. 6 (2004) 299–303. https://doi.org/10.1002/ADEM.200300567.

[103] Y. Gao, Y. Liu, H. Yu, D. Zou, High-entropy oxides for catalysis: Status and perspectives, Appl Catal A Gen. 631 (2022). https://doi.org/10.1016/j.apcata.2022.118478.

[104] A. Sarkar, Q. Wang, A. Schiele, M.R. Chellali, S.S. Bhattacharya, D. Wang, T. Brezesinski, H. Hahn, L. Velasco, B. Breitung, High-Entropy Oxides: Fundamental Aspects and Electrochemical Properties, Advanced Materials. 31 (2019). https://doi.org/10.1002/adma.201806236.

[105] S. Akrami, P. Edalati, M. Fuji, K. Edalati, High-entropy ceramics: Review of principles, production and applications, Materials Science and Engineering R: Reports. 146 (2021). https://doi.org/10.1016/j.mser.2021.100644.

[106] B.S. Murty, J.W. Yeh, S. Ranganathan, P.P. Bhattacharjee, A brief history of alloys and the birth of high-entropy alloys, High-Entropy Alloys. (2019) 1–12. https://doi.org/10.1016/B978-0-12-816067-1.00001-1.

[107] A. Sarkar, Q. Wang, A. Schiele, M.R. Chellali, S.S. Bhattacharya, D. Wang, T. Brezesinski, H. Hahn, L. Velasco, B. Breitung, High-Entropy Oxides: Fundamental Aspects and Electrochemical Properties, Advanced Materials. 31 (2019). https://doi.org/10.1002/adma.201806236.

[108] X. Huang, G. Yang, S. Li, H. Wang, Y. Cao, F. Peng, H. Yu, Noble-metal-based high-entropy-alloy nanoparticles for electrocatalysis, Journal of Energy Chemistry. 68 (2022) 721–751. https://doi.org/10.1016/j.jechem.2021.12.026.

[109] Y. Pan, J.X. Liu, T.Z. Tu, W. Wang, G.J. Zhang, High-entropy oxides for catalysis: A diamond in the rough, Chemical Engineering Journal. 451 (2023). https://doi.org/10.1016/j.cej.2022.138659.

[110] B.L. Musicó, D. Gilbert, T.Z. Ward, K. Page, E. George, J. Yan, D. Mandrus, V. Keppens, The emergent field of high entropy oxides: Design, prospects, challenges, and opportunities for tailoring material properties, APL Mater. 8 (2020) 040912. https://doi.org/10.1063/5.0003149.

[111] P.B. Meisenheimer, J.T. Heron, Oxides and the high entropy regime: A new mix for engineering physical properties, MRS Adv. 5 (2020) 3419–3436. https://doi.org/10.1557/ADV.2020.295/METRICS.

[112] Y. Sun, S. Dai, High-entropy materials for catalysis: A new frontier, Sci Adv. 7 (2021). https://doi.org/10.1126/SCIADV.ABG1600/ASSET/0B8BA449-7251-4A98-A8C7-157A2A1571C6/ASSETS/GRAPHIC/ABG1600-F6.JPEG.

[113] Alloyed pleasures: Multimetallic cocktails | Scinapse, (n.d.). https://www.scinapse.io/papers/41078916 (accessed February 5, 2023).

[114] L. Shao, H. hui Jiang, C. ren Xu, N. Ding, B.Y. Tang, The lattice distortion, mechanical and thermodynamic properties of A(Zr0.2Sn0.2Ti0.2Hf0.2Nb0.2)O3 (A = Sr, Ba) high-entropy perovskite with B-site disorder: First principles prediction, Mater Des. 224 (2022) 111308. https://doi.org/10.1016/J.MATDES.2022.111308.

[115] Y. Pan, J.X. Liu, T.Z. Tu, W. Wang, G.J. Zhang, High-entropy oxides for catalysis: A diamond in the rough, Chemical Engineering Journal. 451 (2023) 138659. https://doi.org/10.1016/J.CEJ.2022.138659.

[116] S. Nie, L. Wu, L. Zhao, X. Zheng, S. Yang, P. Zhang, Entropy-driven chemistry reveals highly stable denary MgAl2O4-type catalysts, Chem Catalysis. 1 (2021) 648–662. https://doi.org/10.1016/J.CHECAT.2021.04.001.

[117] P. Wu, W. Zhu, B. Dai, Y. Chao, C. Li, H. Li, M. Zhang, W. Jiang, H. Li, Copper nanoparticles advance electron mobility of graphene-like boron nitride for enhanced aerobic oxidative desulfurization, Chemical Engineering Journal. 301 (2016) 123–131. https://doi.org/10.1016/J.CEJ.2016.04.103.

[118] C. Riley, A. de la Riva, J.E. Park, S.J. Percival, A. Benavidez, E.N. Coker, R.E. Aidun, E.A. Paisley, A. Datye, S.S. Chou, A high entropy oxide designed to catalyze CO oxidation without precious metals, ACS Appl Mater Interfaces. 13 (2021) 8120–8128. https://doi.org/10.1021/ACSAMI.0C17446/SUPPL_FILE/AM0C17446_SI_001.PDF.

[119] H. Chen, K. Jie, C.J. Jafta, Z. Yang, S. Yao, M. Liu, Z. Zhang, J. Liu, M. Chi, J. Fu, S. Dai, An ultrastable heterostructured oxide catalyst based on high-entropy materials: A new strategy toward catalyst stabilization via synergistic interfacial interaction, Appl Catal B. 276 (2020) 119155. https://doi.org/10.1016/J.APCATB.2020.119155.

[120] H. Xu, Z. Zhang, J. Liu, C.L. Do-Thanh, H. Chen, S. Xu, Q. Lin, Y. Jiao, J. Wang, Y. Wang, Y. Chen, S. Dai, Entropy-stabilized single-atom Pd catalysts via high-entropy fluorite oxide supports, Nat Commun. 11 (2020). https://doi.org/10.1038/S41467-020-17738-9.

[121] H. Chen, J. Fu, P. Zhang, H. Peng, C.W. Abney, K. Jie, X. Liu, M. Chi, S. Dai, Entropy-stabilized metal oxide solid solutions as CO oxidation catalysts with high-temperature stability, J Mater Chem A Mater. 6 (2018) 11129–11133. https://doi.org/10.1039/C8TA01772G.

[122] M. Braic, V. Braic, M. Balaceanu, C.N. Zoita, A. Vladescu, E. Grigore, Characteristics of (TiAlCrNbY)C films deposited by reactive magnetron sputtering, Surf Coat Technol. 204 (2010) 2010–2014. https://doi.org/10.1016/J.SURFCOAT.2009.10.049.

[123] S. Jiang, L. Shao, T.W. Fan, J.M. Duan, X.T. Chen, B.Y. Tang, Elastic and thermodynamic properties of high entropy carbide (HfTaZrTi)C and (HfTaZrNb)C from ab initio investigation, Ceram Int. 46 (2020) 15104–15112. https://doi.org/10.1016/J.CERAMINT.2020.03.045.

[124] T. Wang, H. Chen, Z. Yang, J. Liang, S. Dai, High-Entropy Perovskite Fluorides: A New Platform for Oxygen Evolution Catalysis, J Am Chem Soc. 142 (2020) 4550–4554. https://doi.org/10.1021/JACS.9B12377/SUPPL_FILE/JA9B12377_SI_001.PDF.

[125] X. Chen, Y. Wu, High-entropy transparent fluoride laser ceramics, Journal of the American Ceramic Society. 103 (2020) 750–756. https://doi.org/10.1111/JACE.16842.

[126] A. Lucca, M. Jacquemet, F. Druon, F. Balembois, P. Georges, P. Camy, J.L. Doualan, R. Moncorgé, High-power tunable diode-pumped Yb^3+:CaF_2 laser, Opt Lett. 29 (2004) 1879. https://doi.org/10.1364/OL.29.001879.

[127] Z. Zhao, H. Chen, H. Xiang, F.Z. Dai, X. Wang, Z. Peng, Y. Zhou, (La0.2Ce0.2Nd0.2Sm0.2Eu0.2)PO4: A high-entropy rare-earth phosphate monazite ceramic with low thermal conductivity and good compatibility with Al2O3, J Mater Sci Technol. 35 (2019) 2892–2896. https://doi.org/10.1016/J.JMST.2019.08.012.

[128] J. Xu, J. Li, D. Xiong, B. Zhang, Y. Liu, K.H. Wu, I. Amorim, W. Li, L. Liu, Trends in activity for the oxygen evolution reaction on transition metal (M = Fe, Co, Ni) phosphide pre-catalysts, Chem Sci. 9 (2018) 3470–3476. https://doi.org/10.1039/C7SC05033J.

[129] J. Gild, J. Braun, K. Kaufmann, E. Marin, T. Harrington, P. Hopkins, K. Vecchio, J. Luo, A high-entropy silicide: (Mo0.2Nb0.2Ta0.2Ti0.2W0.2)Si2, Journal of Materiomics. 5 (2019) 337–343. https://doi.org/10.1016/J.JMAT.2019.03.002.

[130] D. Liu, Y. Huang, L. Liu, L. Zhang, A novel of MSi2 high-entropy silicide: Be expected to improve mechanical properties of MoSi2, Mater Lett. 268 (2020) 127629. https://doi.org/10.1016/J.MATLET.2020.127629.

[131] M. Hulko, I. Hospach, N. Krasteva, G. Nelles, Cytochrome C biosensor-A model for gas sensing, Sensors. 11 (2011) 5968–5980. https://doi.org/10.3390/S110605968.

[132] D.H. Gonzalez, X.M. Kuang, J.A. Scott, G. Olimpio De La Rocha, S.E. Paulson, The Terephthalate Probe for Hydroxyl Radicals: Yield of 2-Hydroxy Terephthalic acid and Transition Metal Interference, (n.d.).

[133] M. Zhu, J. Lu, Y. Hu, Y. Liu, S. Hu, C. Zhu, Photochemical reactions between 1,4-benzoquinone and O2•−, Environmental Science and Pollution Research. 27 (2020) 31289–31299. https://doi.org/10.1007/S11356-020-09422-8/FIGURES/7.

[134] Y. Zhang, D. Kudriashov, L. Pershina, A. Offenhäusser, Y. Mourzina, Intrinsic Multienzyme-like Activities of the Nanoparticles of Mn and Fe Cyano-Bridged Assemblies, Nanomaterials. 12 (2022). https://doi.org/10.3390/nano12122095.

[135] C. Cano-Raya, M.D. Fernández Ramos, L.F. Capitán Vallvey, O.S. Wolfbeis, M. Schäferling, Fluorescence quenching of the europium tetracycline hydrogen peroxide complex by copper (II) and other metal ions, Appl Spectrosc. 59 (2005) 1209–1216. https://doi.org/10.1366/000370205774430945.

[136] W.M. Schaffer, T. v. Bronnikova, Peroxidase-ROS interactions\, Nonlinear Dyn. 68 (2012) 413–430. https://doi.org/10.1007/S11071-011-0314-X/METRICS.